Analysing Airborne Optical Remote Sensing Data from a Hyperspectral Scanner and Implications for Environmental Mapping and Monitoring

- results from a study of *casi* data and Danish semi-natural, dry grasslands

PhD thesis

Analysing Airborne Optical Remote Sensing Data from a Hyperspectral Scanner and Implications for Environmental Mapping and Monitoring

- results from a study of *casi* data and
Danish semi-natural, dry grasslands

PhD thesis
2000

Anne Jacobsen
National Environmental Research Institute
Department of Landscape Ecology

University of Copenhagen
Institute of Geography

Data sheet

Preface

The work included in this Ph.D. thesis was performed at the National Environmental Research Institute (NERI)[1], Department of Landscape Ecology, Kalø, the Institute of Geography, University of Copenhagen and at the Center for the Study of Earth from Space (CSES), University of Colorado at Boulder, USA. The study was granted in September 1994 by the Danish Research Council and NERI within the framework of the DANish Multisensor Airborne Campaign (DANMAC) financed by the Danish Space Board. The supervisors were Associate Professor Birger U. Hansen (Institute of Geography, University of Copenhagen) and Senior Researcher Geoff Groom (NERI, Kalø). The thesis work includes a synopsis (Section 1) and a set of publications (Section 2) comprising two proceeding papers and three refereed journal articles.

I greatly acknowledge my supervisors for their support during the Ph.D. programme. I acknowledge Birger Hansen for adding scientific discussions and support especially with regard to fieldwork and for his handling of administrative and economic issues. Geoff Groom has taught me a lot about 'do'es and don'ts' in the world of research and I am thankful to him for scientific discussions as well as improvement of my written English.

The DANMAC project group was the silver cord of my project and I kindly acknowledge all the members of the group. Participation in DANMAC introduced me to most of the national expertise in remote sensing and enabled valuable joint ventures between different scientific disciplines of high value to the thesis work. In the first years, I made an effort to understand radar data and I acknowledge the Danish Center for Remote Sensing and Associate Professor Henning Skriver (Department of Electromagnetic Systems, Technical University of Denmark) for their support. Associate Professor Allan A. Nielsen (Institute of Mathematical Modelling, Technical University of Denmark) improved my grasp on statistics and Scientists Niels Broge (Research Center Foulum) and Michael Stjernholm (NERI, Silkeborg) have been very supportive both scientifically and personally. I would also like to acknowledge other colleagues at NERI, in particular Researcher Rasmus Ejrnæs (NERI, Kalø), who increased my knowledge in vegetation ecology and field botanists Thorsten Krienke and Roar Poulsen.

My stay at CSES gave me a launch-pad when it came to hyperspectral image processing. I am most grateful to the CSES Director Professor Alex Goetz and his staff for welcoming me as a visiting scientist and as part of the staff and I especially thank Scientist Kathy Heidebrecht for her experienced support on atmospheric modelling. I am also thankful to Senior Researchers Joe Boardman and Fred Kruse (Research Systems Incorporated, Boulder, USA) for discussing my data with me. My stay at CSES was only possible due to the support from my family and I thank Jens and Karina for travelling with my children and me.

The PhD program was from an early point scheduled to run for 3½ years from September 1994 to February 1998 thereby reducing weekly working hours to allow for an academic career and a balanced life for a family geographically split between Copenhagen and Jutland. Maternity leave of one year and two periods of three months employment, with the Institute of Geography, University of Copenhagen, and NERI added another eighteen months. The Institute of Geography, University of Copenhagen, awarded the thesis the Ph.D. degree the 26 June 2000.

---

[1] In Danish: Danmarks Miljøundersøgelser, DMU

List of abbreviations

AVIRIS	=	Airborne Visible Infrared Imaging Spectrometer
ATREM	=	Atmospheric REMoval – a programme for atmospheric modelling
BRDF	=	Bi-directional Reflectance Distribution Function
casi	=	Compact Airborne Spectrographic Imager
CDA	=	Canonical Discriminant Analysis
CEM	=	Constrained Energy Minimisation
CEOS	=	Committee on Earth Observation Satellites
CSES	=	Center for the Study of Earth from Space, University of Colorado, Boulder, USA
DANMAC	=	DANish Multisensor Airborne Campaign
DCA	=	Detrended Correspondance Analysis
DGPS	=	Differential Global Positioning Systems
DEM	=	Digital Elevation Model
DN	=	Digital Number
Fl class	=	Floristic class
FOV	=	Field of View
FWHM	=	Full Width at Half Maximum
GCP	=	Ground Control Points
GER2100	=	A field spectrometer from Geophysical Environmental Research
GIS	=	Geographic Information System
IFOV	=	Instantaneous Field of View
ILS	=	Incident Light Sensor
ITE	=	Institute of Terrestrial Ecology, Monkswood, U.K.
J-M	=	Jeffries-Matusita distance
KGRASS	=	The spectral configuration of spatial mode data
LAI	=	Leaf Area Index
Ma class	=	Management class
MaFl class	=	Management and floristic class
MAF	=	Minimum/Maximum Autocorrelation Factor
MIR	=	Middle infrared part of the solar spectrum (1.3 – 2.5 µm)
MNF	=	Minimum Noise Fraction
MODTRAN	=	A program for atmospheric modelling
NASA	=	National Aeronautics and Space Administration, USA
NERI	=	National Environmental Research Institute
NIR	=	Near-InfraRed part of the solar spectrum (0.7 – 1.3 µm)
nm	=	nanometer (0.001 µm)
PCA	=	Principal Component Analysis
PDF	=	Probability Density Function
PPI	=	Pixel Purity Index
SAM	=	Spectral Angle Mapper
SMA	=	Spectral Mixture Analysis
SWIR	=	ShortWave Infrared part of the solar spectrum (0.7 – 2.5 µm)
SPOT HRV	=	Satellite Probation Satellite Terrain, High Resolution Visible
TM	=	Thematic Mapper
TIN	=	Triangulated Irregular Networking
VIS	=	VISible part of the solar spectrum (0.3 – 0.7 µm)
VNIR	=	Visible and Near-InfraRed part of the solar spectrum (0.3 – 1.3 µm)

Content

1. Synopsis

1.1 Introduction

The synopsis begins with this introduction section including a brief overview of the development of imaging spectrometry, a general introduction to data acquired with imaging spectrometers, the so-called hyperspectral data, and an introduction to hyperspectral image data analysis. This is presented as the background for advancement of the hypotheses relevant to the thesis objective, which are also presented in this introduction section. Theoretical sections 1.2 and 1.3 follow, with presentation of the background for the methods developed on the basis of the advanced hypotheses. Sections 1.4 and 1.5 introduce the study area and describe the data collection and data used in the thesis. The contents of the articles relevant to the hypotheses are presented in summary in Section 1.6. The summaries of these articles are, in some cases, presented slightly different from the approach in the articles to stress the parts of specific interest to the actual hypotheses of this thesis. Finally, the synopsis discusses the work presented in Section 1.6 (Section 1.7) and draws conclusions of concern to the thesis objective (Section 1.8).

1.1.1 Brief overview of the development of imaging spectrometry

Earth resources remote sensing of multi-spectral data was initiated with Landsat 1, launched by NASA (National Aeronautics and Space Administration, USA) in 1972 (Curran, 1984). Field, laboratory and multi-band airborne spectrometry development, in particular within geological science, led to increasing recognition of the value of spectral information for Earth resources remote sensing and to the concept of imaging spectrometry (see Section 1.1.2 for definition). The first airborne system was the Airborne Imaging Spectrometer (AIS), available from 1983 (Vane and Goetz, 1993). AIS was a proof-of-concept instrument that led to the development of the AVIRIS (Airborne Visible/Infrared Imaging Spectrometer) – the first airborne scanner to contiguously cover the solar range from 0.4 – 2.5 μm with narrow bands, which was operational from 1989 (Vane et al., 1993). Several imaging spectrometers or hyperspectral scanners are now available (see Table 1 for examples).

Year	Name	Acronym
1983	Airborne Imaging Spectrometer	AIS
1986	(Geophysical and Environmental Research) Imaging Spectrometer	GERIS
1987	(Airborne Visible/Inrared Imaging Spectrometer	AVIRIS
1989	Compact Airborne Spectrographic Imager	*casi*
1994	Hyperspectral Digital Imagery Collection Experiment	HYDICE
1994	Multispectral Inrared and Imaging Spectrometer	MIVIS
1994	Digital Airborne Imaging Spectrometer	DAIS
1997	HYperspectral MAPping	HYMAP

Table 1: Major airborne hyperspectral sensors[*].

The early research work with hyperspectral data was difficult to apply due to **i)** lack of adequate calibration and knowledge of atmospheric effects in order to transform data to surface reflectance, and **ii)** lack of analysis tools to enable the earth scientist to work with the data (Vane and Goetz, 1993). These issues have, to a large extent, been overcome and different methods and image processing systems for calibration and analysis of hyperspectral image data are now available.

Space-based imaging spectrometry represents the next advance in optical Earth Observation data. In 1997 Lewis, a satellite carrying an imaging spectrometer, was launched but never reached orbit. MERIS (Medium Resolution Imaging Spectrometer) was scheduled to be launched by ESA (European Space Agency) in 1999 and in 2000 ARIES (Australian Resource Information and Environment Satellite), another spaceborne imaging spectrometer, is to be launched. NASA will be launching the ASTER (Advanced Spaceborne Thermal Emission and Reflection Radiometer) satellite also in 2000.

1.1.2 Definition of hyperspectral image data

Hyperspectral images are defined as being recorded simultaneously in many, narrow, contiguous bands to provide information on the major features of the spectral reflectance of a given object (Vane and Goetz, 1993). The images can be visualised as a 3-dimensional data set with two spatial and one spectral dimension and the data set is therefore often referred to as an image cube. In addition to contiguous spectral sampling, *hyperspectral* literally refers to data that are (spectrally) oversampled (hyper meaning 'more-than-enough' [Boardman, 1995]) indicating that there are more spectral bands than there are spectral dimensions in the image. Contiguous spectral sampling and spectral oversampling are in contrast to the essential sensing characteristics of the earlier, well established, broad-band *multi-spectral* remote sensing satellite imaging systems such as Landsat TM and SPOT HRV. Image data from these sensors have more spectral variation than the limited number of discrete bands can adequately resolve for. In contrast to these, hyperspectral data provide detailed information on the emission, absorption and reflectance features of the spectral reflectance of a given object. Laboratory work has shown that a spectral resolution of 20 nm and a spectral resampling of at least 10 nm (see Section 1.2.1 for definition) is sufficient for spectral identification of most Earth materials (Goetz and Calvin, 1987). Detailed spectral information like this allows for targets to be determined from their spectral signature, for targets to be identified at a sub-pixel level and – of course – for more traditional remote sensing methods to be used for new applications.

It is considered appropriate at this stage to touch upon the question of whether image data of the present study are actually hyperspectral. Two images acquired with the *casi* (Compact Airborne Spectrographic Imager) were studied. The spatial mode image data consisted of 11 discrete bands of approximately 10 nm spectral resolution; the spectral mode image data were contiguously sampled to 96 bands with a spectral resolution of 5.8 nm and a spectral sampling of 5.4 nm (see Sections 1.2.1 and 1.5.3 for definitions and more details on spectral configurations [Tables 3 and 4]). From the definition given on hyperspectral data, the spectral mode data were hyperspectral whereas the spatial mode data were not. However, the spatial data were of fine spectral resolution including information of not only reflection but also absorption features and hyperspectral image analysis methods as well as traditional classification methods have been applied in the study of these data.

1.1.3 Hyperspectral image analysis

Airborne hyperspectral image analysis can be considered as a three-step process comprising **i)** calibration of image data, **ii)** development of methods for image analysis, and **iii)** georeferencing of the end product (Rubin, 1997). These steps are discussed in the following sub-sections with parallels and differences drawn to satellite multi-spectral remote sensing image data. It will be noted that in work with airborne hyperspectral data greater concern is given to the calibration and georeferencing steps of the analysis. However, a variety of methods are available to overcome these issues, and when the methods have been successfully applied, the hyperspectral data are considered to provide image analysis superior to multi-spectral data. The current section is considered as an overview and introduction to hyperspectral image analysis with more details comprised in Sections 1.2 and 1.3.

Calibration of image data

Calibration of image data is a widely used term referring to different levels of transformation from digital numbers (DNs) to reflectance. A full image calibration optimally includes the radiometric sensor calibration from DN values to at-sensor radiance, corrections for system distortions, transformation of the at-sensor radiance to apparent surface reflectance (atmospheric calibration) and solar and topographic correction to absolute surface reflectance (see e.g. Schowengerdt, 1997).

Sensor calibration
System distortions due to sensor calibration occur in multi- as well as hyperspectral data. System distortions are of more concern when using hyperspectral data since on account of the low signal, the narrow bands require high precision and accuracy in the spectral calibration as well as sensitive detectors that are well calibrated radiometrically. System distortions depend on the quality of the radiometric and spectral calibration of the detectors and on scanner type. The quality of the radiometric and spectral calibration is assessed in this study (Jacobsen et al., 2000a) and system distortions and calibrations are further described in Section 1.2.1.

Atmospheric calibration
As with sensor calibration, the issue of atmospheric calibration is of more concern when using hyperspectral data. Multi-spectral sensors, such as the Landsat TM and SPOT HRV satellite-borne systems, are spectrally configured specifically to avoid the deep absorption features by exploiting the 'atmospheric windows', which are the regions in the solar spectrum outside the main water vapour absorption regions. Hyperspectral images are recorded in a set of contiguous bands and accordingly also in the regions outside the 'atmospheric windows'. This makes atmospheric calibration of hyperspectral data essential but also superior since estimation of the water vapour content is possible from the image data themselves based on the attenuation of radiation. Another method for atmospheric calibration is the use of empirically based models that make use of ground reference reflectance spectra for normalisation of image data without the explicit use of atmospheric models. In the case of either approach, successful atmospheric calibration depends on a good spectral and radiometric sensor calibration. The image analysis in this study is performed on data calibrated to apparent surface reflectance (Jacobsen et al. 2000a) and atmospheric distortions and calibration is further discussed in Section 1.2.2.

Illumination and topographic calibration

Calibration for variations in incident solar radiance due to topography may be performed using digital elevation models (DEM) (Jacobsen et al., 1993). At a national level these may be non-existing or not accurate and precise enough to be valid for application with either airborne or satellite-borne data. The effect of topographic variation is large in airborne hyperspectral data due to the comparatively low altitude of the aircraft platform. The effect is further influenced by the large field of view (FOV) of many airborne scanners, which causes increase in pixel-size towards the lateral extremes of the scan line – a distortion that is superimposed on the topographic displacement of the pixel. This has radiometric consequences as well as consequences for the bi-directional reflectance distribution function (BRDF), which describes the view and illumination angle effects on reflectance (Deering, 1989). The effect also occurs in multi-spectral satellite images and band ratios such as RVI[2] and NDVI[3] (Rouse et al., 1974) have been developed to suppress topographic variation. However, these methods do not exploit the full spectral range of a hyperspectral image and other methods have been developed to suppress image variation due to illumination and viewing geometry for these data (see the following section). The image data used in the study were not calibrated for variation in incident solar radiance due to topography since a DEM was first available only late-on in the study. Analysis of radiometric distortions due to topography and variation in BRDF are therefore not included as such in this study; their effects have been taken into consideration in the section of discussion of results and research methods (Section 1.7).

Image analysis methods

Analysis based on hyperspectral data is fundamentally different from that of multi-spectral data such as the data from Landsat TM and SPOT HRV. This is because the high spectral resolution data allows for deterministic approaches and convex geometry methods as opposed to the more statistic approaches of multi-spectral data (Vane and Goetz, 1993). The statistical approaches of traditional remote sensing techniques are, however, also applicable to hyperspectral data that may be analysed with other methods than those that have been explicit designed to work with this type of data.

The hyperspectral methods for identification and mapping of target materials are designed for use with high quality image data that are well calibrated for atmospheric affects. The methods consider in particular the excess number of bands, the effect of this in terms of both signal and noise and the angular effects of reflectance superimposed onto the derived apparent surface reflectance.

The methods described below are mainly focused on image analysis of relevance to the objective of the study i.e. spectral identification and mapping. Traditional, multi-spectral, as well as hyperspectral methods are described only briefly here and in more detail in Section 1.3.

Statistical methods

Methods for image analysis based on estimation of the covariance matrix are well established in multi-spectral satellite remote sensing and are also a valid means for image analysis in hyperspectral remote sensing. In multi-spectral remote sensing analysis it may be

---

[2] $RVI = R_{NIR}/R_{RED,}$
[3] $NDVI = (R_{NIR} - R_{RED})/R_{NIR} + R_{RED})$
($_{NIR}$ = the near-infrared spectral region; $_{RED}$ = the red spectral region)

6

the case that image analysis is based upon a transformed data set in order to remove correlation between bands. In hyperspectral work transformation to remove correlation is essential. Correlation between bands may be due to topographic shading (leading to a band-to-band correlation), similar target reflectance across a number of bands, or sensor band overlap. Transformation for data reduction often uses principal component analysis (PCA) (see e.g. Richards, 1993), which removes any correlation in the original data and compresses image variance into fewer dimensions. The PCA transforms the data into a new set of variables (Principal Components, PCs). The first PC contains the maximum variance for any linear combination of the original bands, the second PC contains the maximum possible variance for any axis orthogonal to the first PC and so on.

Hyperspectral data are often influenced by system distortions since the high spectral resolution sets high demands with respect to sensor calibration and the signal-to-noise ratio. In the hyperspectral case, feature extraction is therefore often based on a noise adjusted principal component transformation, known as the minimum noise fraction (MNF) transformation (Green et al., 1988) or the equivalent Minimum/Maximum Autocorrelation Factors (MAFs) approach (Conradsen et al., 1991). The MNF/MAF transformation is essentially a noise adjusted principal component transform that is especially valid in the hyperspectral case since the transformed bands are ordered with respect to image quality, with the noisier bands being the higher order bands. These transformations perform a better noise separation than PCA (the transformations are spatially based and therefore superior for image analysis) and since the noise is isolated in the higher order bands visual inspection of the feature images is facilitated (Conradsen et al., 1991).

Traditional spectral classification
Traditional multi-spectral classification such as supervised Maximum Likelihood (ML) classification is dependent on good training classes; this means, from a statistical point of view, that there must be a significant number of pixels to describe the spectral signature of each class and that the spectral classes must be well separated. In the case of ML classification, Swain and Davis (1978) recommend 10 to 100 pixels per class per feature for proper statistics to be performed. ML classification of hyperspectral data therefore relies on a larger number of training pixels for proper results to be obtained, and the increased information in the covariance matrix of hyperspectral images is to some extent traded-off by the required large size of the class training data sets. However, methods of region growing (Nielsen et al., 1998) may overcome this issue by increasing number of pixels in the training class.

Spectral matching
Spectral mapping based on the comparison/matching of individual image spectra to a spectral library of ground or laboratory based spectral signatures is an option that is unique for hyperspectral data. The following are examples of spectral mapping methods that normalise albedo variations due to illumination and view angle geometry before matching.

Binary encoding followed by *spectral matching* to a spectral library that has been equally encoded is a simple method that is sensitive to band positions but insensitive to albedo variations (Kruse et al., 1993a). Binary encoding encodes the data and reference spectra into 0s and 1s dependent on whether bands lie below or above the spectrum mean. *Continuum removal* is another means of normalising apparent surface reflectance. This allows for comparison of individual absorption features from a common base line (Kruse et al., 1993a). *Spectral angle mapper* (SAM) matches image spectra to reference spectra in n-dimensions by comparing the angle between a reference spectrum considered as an n-dimensional vector (n

being number of bands) and each pixel vector in n-dimensional space (Kruse et al., 1993b). This spectral angle distance is independent of the magnitude of the spectral vectors and therefore insensitive to illumination and view angel variations (Kruse et al., 1993b).

Spectral mixture analysis
One other way of analysing pixel spectra of multi-spectral as well as hyperspectral images has been based on the general concept that pixels are not really pixels but 'mixels' – a mixture of the ground target reflectances within a single pixel. Spectral mixing occurs at any pixel resolution and any spectral resolution. Due to the high spectral resolution of hyperspectral data, they have important implications for spectral unmixing in terms of identification of target materials at a sub-pixel level and determination of the relative abundance of the pure components/targets in an image. The pure targets that make up the spectral mixture of a given image are called the image endmembers. Full unmixing is an attempt to linearly unmix all spectral endmembers in an image (Kruse et al., 1993, Gamon et al., 1993 and Wessman et al., 1997). Partial unmixing is an attempt to map one or more target endmembers without knowledge of the full number of endmembers and is a valid method if only a few targets are of interests (Goetz et al., 1996, Boardman et al., 1995).

Two examples of image analysis methods are shown in this study. The first is based on partial unmixing of the image data (Jacobsen et al., 1998); the second is based on statistical methods and traditional maximum likelihood classification (Jacobsen et al., 2000b) .

Georeferencing

Georeferencing of airborne data is of concern as in the case of satellite borne data. It is important for further application of the remote sensing products in, for example, geographic information systems (GIS) and for the analysis process itself if ground sampling is applied for supervised analysis or classification.

There are, however, special concerns for georeferencing of airborne data due *inter alia* to aircraft attitude variations (pitch, yaw and roll). Parameters mentioned as important for topographic correction of the signal (increased topographic effects due to low platform attitude and across track variation in pixel-size due to large FOV) are also of importance for georeferencing. Polynomial distortion models have traditionally been used for satellite images. Poor model correspondence in one area (i.e. high residual errors) may be improved by adding more ground control points (GCPs) to the distortion model. This will, however, most likely merely move the area of weak correspondence to somewhere else. Triangulation is an alternative to polynomial distortion modelling. With this method, poor correspondence in one area may be improved by adding a new GCP without affecting the modelling of other areas. Both polynomial and triangulation methods may be further refined to account for topography and scan geometry. However, the models do not have the capability to model the unsystematic variations of an unstable airborne platform and piecewise triangulation has been suggested to overcome the problem (Devereux, 1990).

The image data of the study were georeferenced (Jacobsen et al., 1999b) for analysing ground based vegetation data with image derived reflectance spectra (Jacobsen et al., 1999a and 2000b).

1.1.4 Objective of the thesis

In 1995, a pilot study of field spectra and vegetation data from old grasslands with high

biodiversity and young, sown grasslands of low biodiversity was performed. This was undertaken to analyse the spectral separation of grasslands based on management in terms of age and vegetation variation in terms of biodiversity (Jacobsen et al., 1995). The promising results of this pilot study initiated this study of airborne hyperspectral data analysis of the vegetation on semi-natural grasslands.

The overall objective of the thesis project has been analysis of airborne optical remote sensing data from a hyperspectral scanner and analysis of implications for encroachment monitoring and plant community mapping of Danish semi-natural, dry grasslands. This has been in order to enlighten the issue of whether remote sensing technologies of today are capable of producing vegetation maps of such a quality and spatial resolution that they are suitable for research and monitoring interests in Denmark.

Thesis work included development of methods for sensor and image calibration issues (Jacobsen et al., 2000a), image analysis of vegetation on semi-natural grasslands using all ready established and explicitly developed methods (Jacobsen et al., 1998, 1999a, and 2000b), and development of methods for georeferencing (Jacobsen et al., 1999b).

Under the headings of the three-step process of airborne hyperspectral image analysis mentioned earlier (Section 1.1.3), the following hypotheses were advanced:

i) data quality assessment and image calibration

> ... the radiometric calibration quality and the spectral wavelength calibration and precision of contiguously sampled image spectra can be assessed from the image data themselves and by atmospheric modelling;

> ... atmospheric calibration can be performed using a linear model based on one light calibration target and atmospheric modelling;

ii) development of image analysis methods

> ... encroachment stage can be monitored at the level of the individual woody species using spectral unmixing;

> ... the source of spectral variation of vegetation within areas of the same management categories can be related to plant species composition;

iii) georeferencing of the end product

> ... automated extraction of an unlimited number of terrain tie points from a high resolution digital elevation model and Triangulated Irregular Network (TIN) resampling can be used to correct for attitude induced terrain effects.

The rationale of the thesis objective

Studies of airborne hyperspectral remote sensing data are of importance for various reasons. In general terms, the present study contributes to **i)** research with relation to remote sensing issues as a test-bed for ground and satellite based remote sensing and **ii)** research with relation to implications issues for monitoring and mapping of semi-natural grasslands and

for integration of ecological and remote sensing data in Danish nature monitoring and research.

Test-bed studies
Airborne remote sensing is valuable as the link and reference between ground and spaceborne data, with results of data analysis contributing to discussion of the design of spaceborne sensors. Further work for evaluation and development of spaceborne sensors are essential for remote sensing as a whole. Airborne scanners offer controlled means to achieve this and to develop data processing and analysis techniques for the next generation of imaging spectrometry from space (Blackburn and Milton, 1997).

Danish nature monitoring and research
Encroachment mapping of semi-natural grasslands is of interest as environmental management of this particular nature type for conservation issues makes use of livestock grazing and mechanical cutting to prevent dense encroachment by woody plant species such as juniper and gorse.

Mapping of plant communities is of interest to on-going succession studies. The Danish semi-natural grasslands vary from highly productive, species poor fallow land to less productive, species rich semi-natural grasslands. Studies of field data have shown that single species respond to predictors such as vegetation cover (trees, herbs, bare soil), pH, soil type, topography and soil moisture (Ejrnæs, 1999) and that they may be modelled from these predictors. Advances in research and development of such models on a landscape level, to predict the occurrence and composition of unimproved grassland vegetation, could potentially be obtained through work with available soil databases, elevation models and remotely sensed data (Ejrnæs, 1999).

Perspectives of airborne data
In a broader perspective, airborne hyperspectral remote sensing is becoming increasingly accessible due to the increasing number of commercial companies operating hyperspectral scanners. Airborne data acquisitions benefit greatly over satellite based missions from being operational in the sense that the user has influence on the mission in terms of flight line position, calibration measurements, spectral resolution, ground resolution, acceptable weather conditions and time schedule (Wilson, 1994).

On the other hand, airborne data from a hyperspectral scanner are, for the individual user of such data often very expensive on account of the limited spatial coverage of an image and the fact that multiple flight lines are often required to cover a study area. Furthermore, there is a limited range of operation associated with issues of aircraft speed and endurance, and data processing for georeferencing and atmospheric correction is complex (Wilson, 1994). Airborne hyperspectral data are therefore, under their current economics, mainly valuable for test-beds studies, implications studies for forthcoming space-borne hyperspectral data (Blackburn and Milton, 1997) and for occasional classification of natural areas for studies of, for example, semi-natural grasslands.

10

1.2 Image distortions in hyperspectral remote sensing data

Section 1.1.3 introduced the processing needs of airborne hyperspectral image data with parallels and differences drawn to spaceborne multi-spectral image data. This section and the following (Section 1.3) will discuss in more detail the theoretical background for understanding and performing the three-step process of airborne hyperspectral image processing and further consideration of the processing of satellite multispectral image data is not made. The three-step process of airborne hyperspectral image processing introduced in Section 1.1.3 comprises **i)** calibration of image data, **ii)** development of methods for image analysis, and **iii)** georeferencing of the end product. This first section describes the characteristics of the system, atmospheric and geometric distortions that have to be accounted for in the calibration of airborne hyperspectral image data and the methods available for undertaking the calibration.

1.2.1 System distortions

System distortions that need to be taken account of in calibration of hyperspectral image data are a result of problems in the sensor calibration, scanner construction and aircraft instability.

Sensor calibration – definitions

The radiometric calibration of a sensor describes the conversion from recorded digital numbers (DNs) to at-sensor radiance in µW/cm²/sr/nm based on instrument gain and intercept. This level of calibration is most often supplied by the operating company and is generally known as Level 1B correction.

The spectral calibration of a sensor (Figure 1) describes **i)** the position of the centre wavelength of the sensor i.e. the wavelength calibration and **ii)** the Full-Width-at-Half-Maximum (FWHM) - i.e. the spectral resolution being the instrument response to a monochromatic source (Curtiss and Goetz, 1994). The spectral resolution (Figure 1) of the instrument is a measure of the narrowest spectral feature that can be resolved by the system. The spacing between sample points in the spectra describes the spectral resampling.
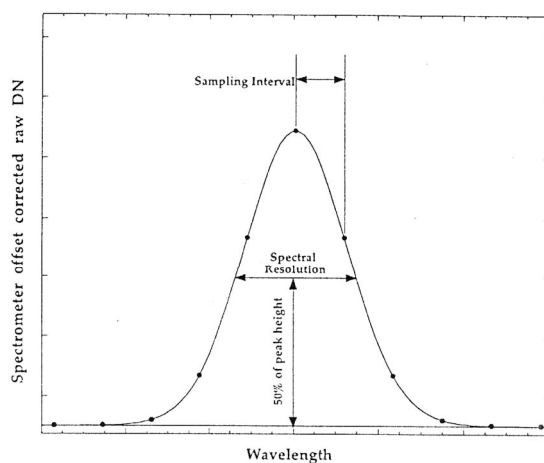
Figure 1: A spectrometers response to a monochromatic source. In this case, the spectral resolution (measured as the FWHM of the feature) is about 2.5 times the spectral sampling interval (for further information see http://www.asdi.com).

Calibration quality

The calibration of the individual sensors in an linear array scanner like the *casi* used in this study is of importance to the quality of parameters derived from the image data. It is of special concern for the retrieval of surface reflectance based on atmospheric modelling that the sensor calibration of a hyperspectral scanner is both stable and accurate.

The determination of surface reflectance depends on the precision and accuracy of the sensor and its calibration. It is important to be aware that as a function of the band width narrow band sensors receive less signal than broad band sensors. The spectral calibration is a matter of the precision of the wavelength calibration and the spectral resolution (FWHM) of a given band. In order to match the slopes of the deep atmospheric water vapour features and other narrow absorption bands such as that of oxygen a precision to the nearest 0.1nm is necessary for an instrument with a 10 nm spectral resolution (Goetz and Heidebrecht, 1996). This is difficult to obtain and for this degree of precision every sensor in a linear array might need its own atmospheric calibration (Goetz and Heidebrecht, 1996).

Noise

Sensor induced noise in an image is a function of the scanner type. The image data of this study were acquired with a linear array scanner. In a linear array scanner variation in calibration between detector elements may be seen as striping along flight lines (Larsen et al., 1998). Another factor causing image noise in linear array scanner data is improper spectral alignment between the entrance slit and rows in the detector array (Goetz and Heidebrecht, 1996), which is seen as a 'spectral smile' or 'twist' across track the image (Figure 2). Linear array scanner data may also be affected by **i)** global noise, i.e. random DN variation in every pixel, caused by electronic variation in the sensing and recording system due to vibrations of the aircraft and **ii)** local noise, i.e. pixel, column or line drop outs caused by data transmission loss or saturation (Larsen et al., 1998). (Periodic noise with a high spatial correlation such as striping or banding only occurs in line and or whiskbroom (e.g. rotating mirror) scanner data [Nielsen and Larsen, 1994]).

Figure 2: Example of wavelength offsets across track. In this case, the data were resampled and the offset recalculated. The expected values represent theoretical restored data (Goetz and Heidebrecht, 1996).

Removing system distortion

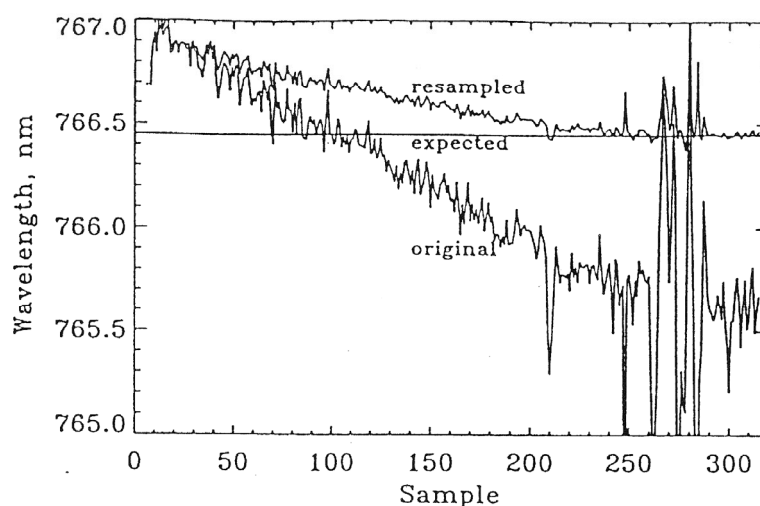Methods for removal of system noise are dependent on the character of the noise. Local noise of single bad lines or columns may be removed relatively simply using convolution filters; however, this has the draw back of also altering other, noise-free, pixels. PCA and MNF/MAF transformation (Section 1.1.3) are other valid ways of detecting all types of image noise whether it is global, local, banding, along or across track striping (Nielsen and Larsen, 1994; Larsen et al., 1998). In either case, the original bands may be restored from the inverse transformation of a set of PCs or MNFs/MAFs either by excluding the noise bands/lines or substituting the noise bands/lines with their mean value (Larsen et al., 1998). In the case of image noise with consistent periodicity (coherent noise), well-defined spikes will occur in a Fourier transform of the noisy image. The relevant spikes may be filtered out before an inverse transformation is performed and coherent noise can be removed in this way (Nielsen and Larsen, 1994).

1.2.2 Atmospheric distortions

Sources of atmospheric distortions

Interpretation of data from remote sensing is complicated by atmospheric effects due to **i)** scattering by dry air molecules and particulate matter (haze) and **ii)** absorption by air molecules. Scattering and absorption both attenuate the transmission of solar radiation through the atmosphere.

The scattering component of the attenuation is the path radiance, which is the amount of radiation that is reflected from the atmosphere to the scanner without any interaction with the ground. Scattering by dry air molecules (Rayleigh scattering) decreases rapidly with wavelength ($\sim \lambda^{-4}$) whereas scattering by particulate matter decreases less rapidly (Iqbal, 1983). Generally speaking, 10% of the radiation measured at 1.0 µm at a satellite is made up of scattered light (Gao et al., 1993) and scattering is therefore mainly important in the shorter wavelengths.

Absorption of solar radiation by air molecules is a selective process that occurs only at discrete wavelengths. The main molecular absorbers in the atmosphere are shown in Figure 3. The atmosphere is seen to be transparent in the visible (VIS) part of the spectrum (0.3 – 0.7 µm) and influenced by molecular absorbers such as water vapour, CO_2 and O_2 in the infrared (IR) part of the spectrum (0.7 – 2.5 µm).

Water vapour is the most variable constituent in the atmosphere. Water vapour absorbs in discrete wavelengths throughout the solar spectrum. The most dominant absorption features associated with water vapour are at 0.94, 1.14, 1.4 and 1.9 µm (Stoner and Resmini, 1996). In the visible and near-infrared (VNIR) spectral region of concern of this study (0.4 – 0.9 µm) minor water vapour absorption features occur at 0.72 and 0.82 µm. Other dominant absorbers of concern in this region are O_2 and O_3. O_2 has a major absorption feature centred at 0.76 µm and two minor absorption features centred at 0.63 and 0.69 µm. O_3 exhibits absorption from 0.45 to 0.77 µm (Figure 4).
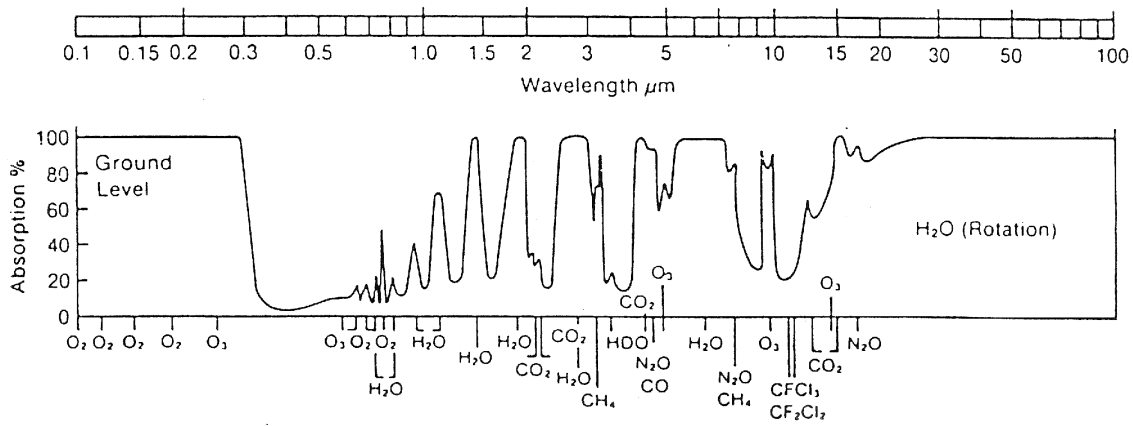
Figure 3: The electromagnetic spectrum from ~0.1μm to 100 μm and atmospheric absorption. (Mitchell, 1989, modified).
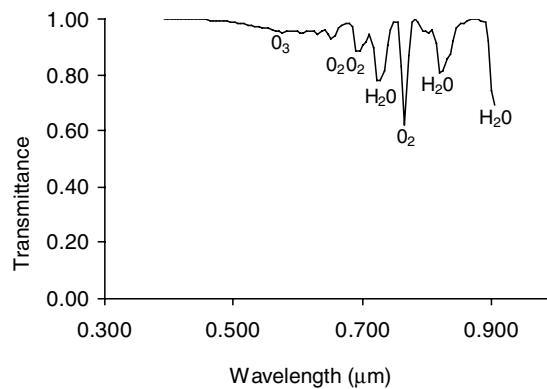
Figure 4: The electromagnetic spectrum from 0.4 to 0.9 μm and atmospheric transmission as modelled with ATREM for the 10th June 1997, the day of image acquisition.

Radiation is attenuated on its way from the sun through the atmosphere to the ground and on its way back to the sensor. The effect of attenuation of up-welling radiation is dependent on the path length as a function of the altitude of the image acquisition platform and the sensor field-of-view (FOV). The combination of a large FOV and a low flying altitude that is commonly the case for airborne platforms affects the path length of the up-welling radiation radically, as a function of the position of the pixel across track. Ideally, atmospheric calibration should account for this effect.

Calibration of atmospheric distortions

There is a special concern for atmospheric calibration of a hyperspectral image because it is a recording of a contiguous spectral radiance. Narrow absorption bands affect the radiance recorded at the sensor dramatically and even small wavelength shifts shift the absorption band of the sensor. Furthermore, attenuation and scattering of the radiance affect the images due to variations in viewing geometry.

14

The modelling approach for atmospheric calibration of hyperspectral images makes use of the image data themselves (Gao et al., 1993; Goetz et al., 1997). ATREM (CSES, 1997) and MODTRAN (Berk et al., 1989) are examples of atmospheric calibration models. ATREM is used for atmospheric calibration in this thesis. It uses a three band ratio within and outside of the water vapour absorption feature to correct for water vapour in the whole spectral region on a pixel-by-pixel basis and a scattering calculation to account for the haze in the atmosphere (Gao et al., 1993). The ATREM atmospheric modelling takes account of the altitude of the acquisition aircraft and differences in attenuation due to water vapour as a function of path length but does not take into account the pixel-based variation in attenuation due to the scattering component.

An alternative approach for atmospheric calibration, the empirical line method (Kruse, 1994; Goetz et al., 1997) is one of several techniques that normalises at-sensor radiance to surface reflectance. It is a linear model based on field measurements of spectral reflectance of a light and a dark object and recorded radiance at the sensor of the same objects. The result is a gain factor for each band that describes the multiplicative influences of atmospheric transmission, solar irradiance and instrument response functions and an off-set that is related to the sensor and the path radiance (Goetz et al., 1997).

The success of both atmospheric calibration and normalisation are dependent upon the radiometric and spectral calibration of the sensor (Section 1.2.1) as both methods involve division of the image data by either modelled surface radiance or measured surface reflectance.

Dwyer et al., (1995) assessed the differences in surface reflectance factors of the modelled and the empirical methods and found that spectral features were somewhat subdued using the modelled based method when compared with those calibrated using the empirical line method. Both methods produced spectra similar to laboratory and field measurements.

The combination method takes advantage of both the modelling and the empirical line method. Application of the empirical line method to model-based apparent surface reflectance factors benefits from being accommodated to the variability of water vapour in the image whilst, at the same time, the apparent surface reflectance factors are normalised to ground spectra (Clark et al., 1995; Goetz et al., 1997).

1.2.3 Geometric distortions

Sources of geometric distortions

Sources of geometric distortions of special concern to airborne scanner data are related to an unstable platform, low acquisition altitude, and large FOV.

Low altitude acquisition combined with the large FOV causes pixels in the nadir line to be smaller than pixel in the edges of the swath due to the panoramic effect (equation 1; Richards, 1993):

$$p_\theta = \beta \, h \, \sec^2 \theta = p \, \sec^2 \theta \qquad\qquad\qquad \text{eq.1}$$

where p_θ is the size of the pixel in a given scan direction at scan angel θ, β is the instantaneous field of view (IFOV, the spatial size of one pixel), h is altitude and p is pixel dimension at nadir. The largest view angle of the image data in this study was 42° (FOV)/2 and with an acquisition

altitude of 1347 m this resulted in $p_\theta = 1.14$ p. This indicated that the geometric distortion at the edge of the swath due to the panoramic effect was 14% causing the nadir pixel size of 2m to increase to 2.3m.

The panoramic effect is further complicated by the topography. The displacement d_x of a pixel is (equation 2; Richards, 1993):

$$d_x = d_z \tan \theta / p_\theta \qquad\qquad \text{equation 2}$$

where d_z denotes the relative height over a selected reference elevation. In the extreme positions across track of the image data of this study, a relative height of 30m will induce a pixel displacement of 5-6m or up to 3 pixels.

The displacement of pixels is further influenced by variation in platform velocity, altitude and attitude due to factors such as atmospheric turbulence. An increase in altitude will change the geometry of the pixel as illustrated in Figure 5(a). Variation in velocity changes the pixel size along track (Figure 5(b)), attitude variation in the forms of pitch, roll and yaw results, respectively, in along track displacement, across track displacement and image rotation (Figure 5(c)-(e)).
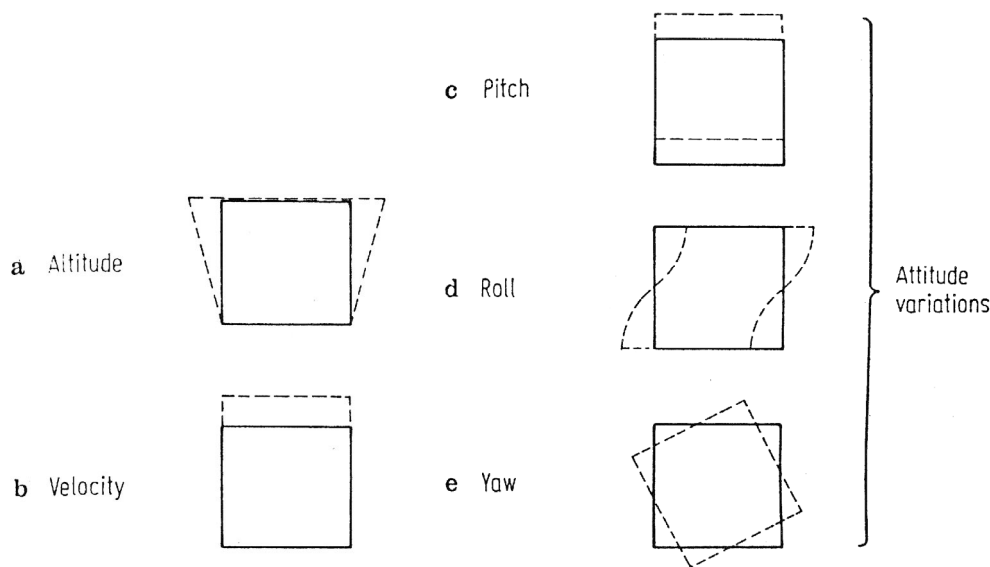
Figure 5: Effects of platform position and attitude errors on the region of the Earth being imaged, when those errors occur slowly compared with image acquisition (Richards, 1993, modified).

Small frames, fast frame acquisition times, low altitude and narrow swath width of airborne scanners means that Earth rotation, causing image-skew and Earth curvature and consequently an increase in pixel size at the edges of the swath are not problems for airborne scanner data.

Georeferencing

Georeferencing is the process of transforming a set of image data from image space to geographical map space by warping the image based on a distortion model, a coordinate transformation and resampling/interpolation (see e.g. Richards, 1993).

The distortion model is the approximation of the coordinate transformation between reference map and input image coordinates estimated from a set of ground control points (GCPs). The distortion model is most often approximated using polynomial functions even though there are a number of disadvantages to be aware of: **i)** the polynomial transformation can only deal with a limited number of smooth changes in image geometry, **ii)** the method does not guarantee a correct transformation at GCP locations, **iii)** GCPs from locally distorted parts of the image may lead to inaccuracies over a wider area (Devereux et al., 1990). GCPs and resampling grids may be corrected for view angle and topographic displacement using digital elevation data but the rapid changes in the image geometry due to aircraft motion/attitude variations cannot be accounted for using global polynomial models.

It was mentioned in Section 1.1 that piecewise distortion modelling is recommended using either polynomial models (Schowengerdt, 1997) or triangulation (Devereux et al., 1990) to account for sensor platform attitude variation. Other methods include use of a three axis stabilised platform mounted on the aircraft to correct for pitch and yaw and a gyro to account for the roll effect (Richards, 1993). Other arrangements include gathering of aircraft motion compensation data as part of an airborne scanning campaign such as several separate antennae for Differential GPS positioning of the aircraft for accurate measure of the attitude (Wilson, 1994).

1.3 Image analysis

The image analysis in this study was developed on the basis of **i)** traditional remote sensing image analysis using supervised maximum likelihood classification and **ii)** spectral mixture analysis applying convex geometry concepts in terms of partial unmixing. This section gives the theoretical background for these methods with regard to work with hyperspectral image data. The section also discusses the spectral reflectance of vegetation and the limitations and possibilities for applying hyperspectral methods in vegetation studies.

1.3.1 Maximum likelihood classification

The performance of supervised maximum likelihood (ML) classification relies on the user-defined training classes. In physical terms, sound training classes are representative of the natural surface they are to represent. In statistical terms, sound training classes should be non-overlapping and spectrally characterised by a Gaussian (normal) distribution of their probability distribution functions (PDFs; Cortijo and Blanca, 1997). The discussion of this section is related to the latter.

The ML classification is based on a particular case of the Bayes rule (see e.g. Richards, 1993) and it is prerequisite from a statistical point of view that the training classes are Gaussian in order to be well described by a vector and the covariance matrix. The quadratic decision boundaries imposed by the ML classifier are more sensitive to violation of the Gaussian assumption and high-overlapping training classes than linear decision boundaries (Cortijo and Blanca, 1997) and special concern should be taken to ensure that the training classes are Gaussian, separable and non-overlapping.

The Jeffries-Matusita (J-M) distance (see e.g. Niblack, 1985) is a valid means of measuring the distance between two classes in a given set of spectral bands to see if training classes are pairwise separable and non-overlapping. The distribution of two hypothetical classes in one dimension is plotted in Figure 6(a), and the J-M distance related to the shaded area is shown in Figure 6(b). The larger the shaded area, the more separable are the two classes. The measure for maximum pairwise separability is bounded by $\sqrt{2}$ (i.e. a value of ~ 1.41).
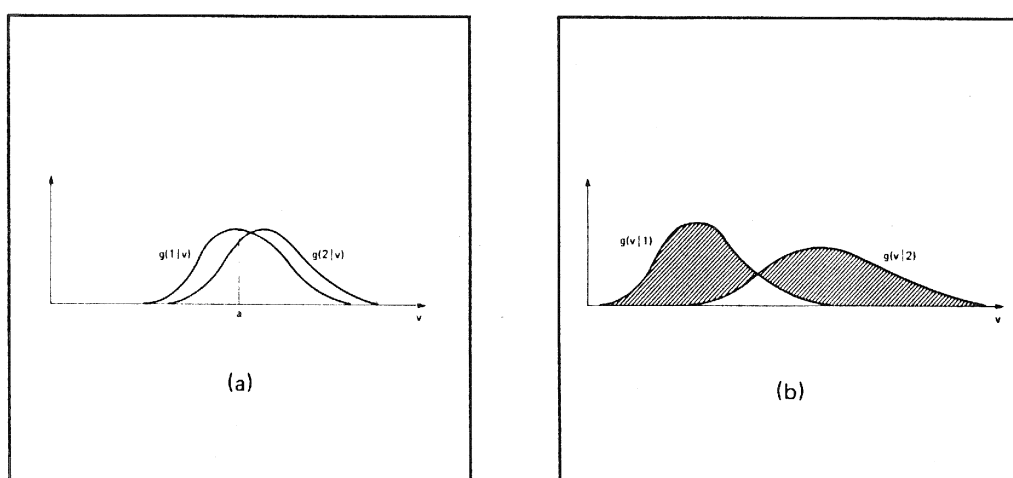
Figure 6: (a) Distributions for two classes with high overlap. A pixel with value 'a' has a high likelihood of belonging to class 1 but may still easily belong to class 2. (b) Distributions for two classes showing the region belonging to the J-M distance (Niblack, 1985).

Canonical discriminant analysis (CDA) (see e.g. Richards, 1993) is a valid means of evaluating if a training class comprises more than one spectral class since, as opposed to the PCA, the CDA is class sensitive. CDA takes into consideration both the mean of the spectral classes and their individual spreads (see Figure 7 for illustration). If the scatterplot of the first two canonical discriminant function forms only one ellipsoid data cloud, the training class is Gaussian and consists of one spectral class only. If the scatterplot forms two data clouds, the training class consists of two spectral sub classes, and so forth.
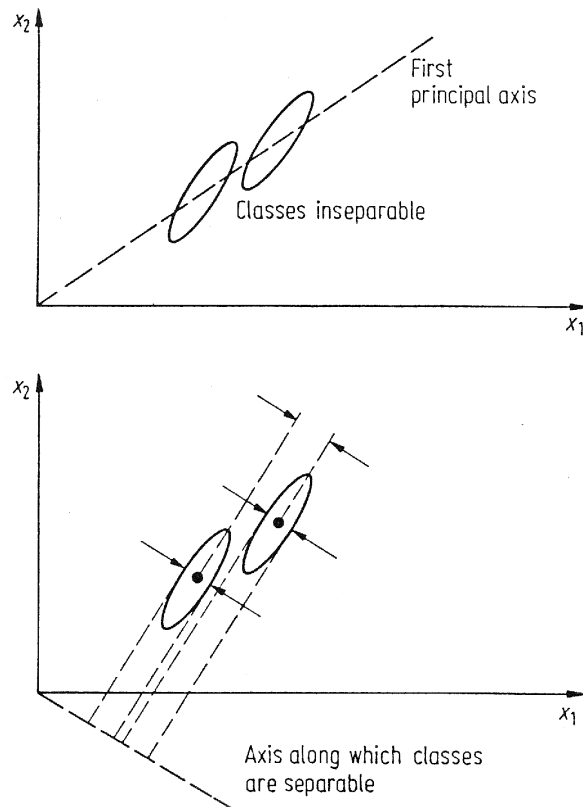
Figure 7: (a) Hypothetical two dimensional, two class data illustrating lack of separability in either the original bands or the principal components; (b) Axis along which classes can be separated (Richards, 1993, modified).

1.3.2 Spectral mixture analysis

The basic idea in a spectral mixture analysis (SMA) is that each pixel is a physical mixture of multiple components weighted by their surface abundance (Tompkins et al., 1997).

Linear mixing

The simplest mixing model describes the mixed pixel as a linear combination of the endmembers (the 'pure' spectra) in the pixel, weighted by their abundance. The linear model can be regarded in terms of physical concepts including the IFOV of the pixel, the incoming radiance, the photon-material interactions and the resulting mixed spectra (Boardman, 1998). More simple and easier to invert is a mathematical model describing the observed spectrum (a vector) as the result of multiplication of the mixing library of endmember spectra (a matrix) by the endmember abundances (Boardman, 1998). Basically speaking, each material (endmember) of a pixel has a unique spectrum, and the mixed spectrum is just weighted average (Figure 8).

20

The linear model is based on the physical concepts that there is no interaction between materials. Boardman (1998) finds this is a valid approach for large scale area mixing whereas others disagree with this and consider that non-linear mixing, in particular, in vegetation studies, is relevant (Ray and Murray, 1996; see Section 1.3.3).

class a: 65% area, spectrum E_a

class b: 20% area, spectrum E_b

class c: 15% area, spectrum E_c
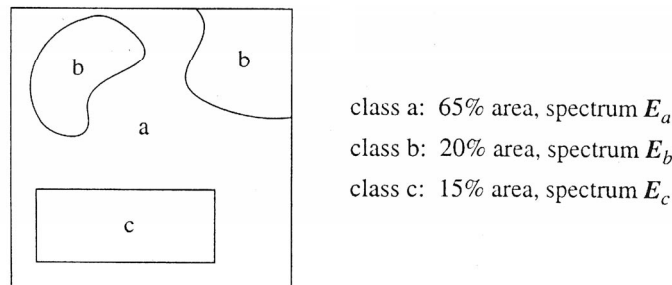
total spectrum at pixel: $DN = 0.65E_a + 0.20E_b + 0.15E_c$

Figure 8: The linear mixing model for a single pixel (Schowengerdt, 1997, modified).

Convex geometry

The linear mixed-pixels problems can be conceptualised in terms of convex geometry. One definition of points in a convex set is that they are positive, unit-sum linear combinations of some fixed points, the vertices of the convex hull of the set (Boardman, 1995).

Figure 9 shows a scatterplot of mixtures of three endmember materials, in this case dark soil, light soil and crop. The corners of the smallest simplex surrounding the convex hull define the outer triangle, the middle triangle is defined by the most extreme pixels along the DN axis, and the inner triangle is defined by supervised class means. It is assumed that all possible mixtures lie within the outer triangle.
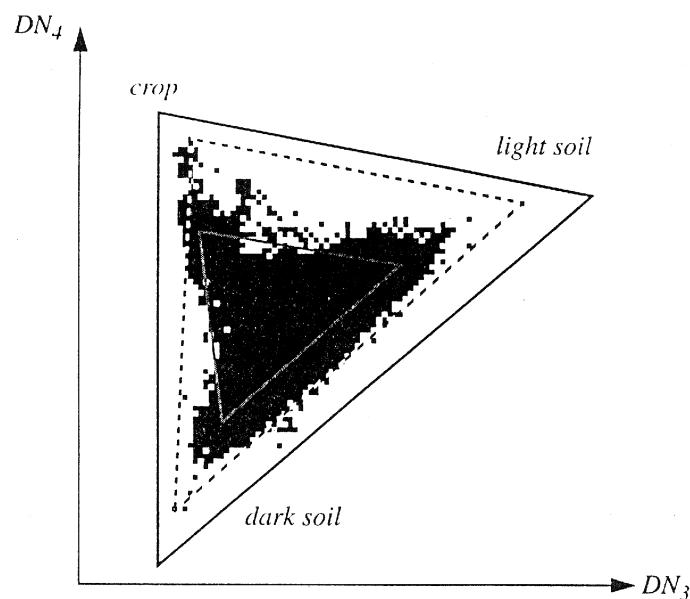
Figure 9: Scatterplot of mixtures of three endmember materials (Schowengerdt, 1997, modified).

The application of convex geometry concepts in unmixing is based on four crucial points (Boardman, 1995): **i)** convex sets have the same definition as mixed pixels; **ii)** feasible mixed spectra are unit-sum, all-positive linear combinations of the pure endmember spectra; **iii)** feasible spectra are interior to the convex hull defined by endmember vertices; and **iv)** the dimensionality of the mixed data is one less than the number of linear dependent endmembers.

Based on these principles, Boardman (1995) proposed an automated method for retrieval of image endmembers from the image itself as opposed to user-defined endmembers. First the data are reduced to apparent surface reflectance; next the data dimensionality is determined using the MNF transformation and third, the endmembers are identified as the corners of the smallest simplex surrounding the convex hull of the data points. Given the constraints that the abundances within every pixel were non-negative and summed to unity, the endmembers are unmixed into abundance maps. This method is reliant on linear mixing only and on knowing all endmembers in the image (full linear unmixing). If only one or two endmembers are desired partial spectral unmixing may be performed (Boardman et al., 1995; Resmini et al., 1997).

Partial spectral unmixing

In order to perform successfully, partial unmixing by Matched Filtering (MF) or Constrained Energy Minimisation (CEM) (Resmini et al., 1997; Goetz et al., 1996) requires that the target of interest is unique compared to the background reflectance (Stoner and Resmini, 1996; Boardman et al., 1995).

CEM maps the targets from their spectral characteristics without knowing the spectral characteristics of the background endmember. The CEM method minimises the variance of the overall spectral response and gives unit scores only to pixels with perfect spectral matches. All other pixels will be nulled and receive a near-zero filter response, except for the undesired endmembers, which are spectrally significant targets without mapping interest that are existing in a limited quantity. These will be mapped as false positives with high abundance scores because they are considered as background even though the targets are endmembers in spectral terms (Jacobsen et al., 1998).

In general, convex geometry concepts and CEM work well when the desired endmembers are the covariance drivers of the image statistics either on account of their number or on account of their spectral characteristics.

1.3.3 Vegetation and remote sensing

It was recognised early-on in the use of remote sensing images that spectral reflectance data were valuable for the modelling of biophysical variables and much research is still developing this application of remote sensing (Jacobsen, 1995; Jacobsen and Hansen, 1996; Gilabert et al., 1996; Goetz, 1997; Tod et al., 1998; Jacobsen and Hansen, 1999). Remote sensing has also found application within vegetation mapping, land cover change detection, disturbance monitoring and the estimation of biochemical as well as biophysical attributes of ecosystems (Curran et al., 1992; Curran et al., 1998; Asner, 1998).

Parameters of spectral reflectance derived from hyperspectral image data, such as absorption feature width, depth and symmetry have been seen to be more sensitive to plant biochemical states than parameters derived from broader band reflectance data (Wessman,

1994; Vane and Goetz, 1993). Hence, new vegetation remote sensing perspectives are being opened with the era of hyperspectral data.

Spectral reflectance of vegetation

The spectral variation of vegetation registered by hyperspectral data (Figure 10) is related to the chemical constituents of plants (Gates et al., 1965; Wooley, 1971), their water status (Peñuelas et al., 1993), cell structure, morphology and tissue constituents (Wessman, 1994).
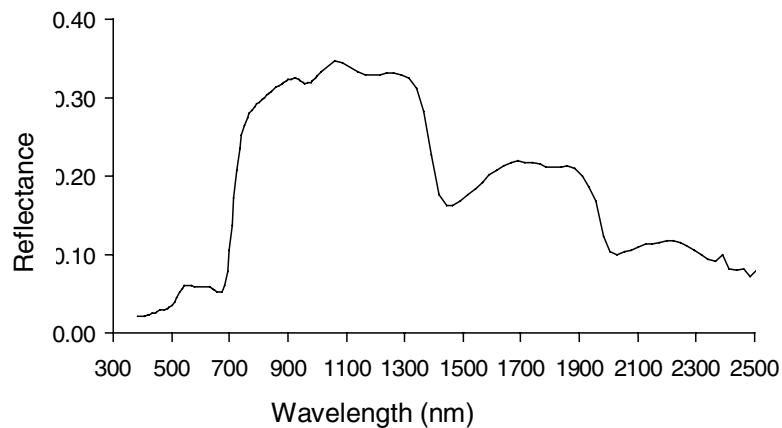
Figure 10: Spectral reflectance of an arbitrary vegetation plot measured during the field campaign in 1997 with GER2100.

Absorption in the visible wavelengths (VIS) (0.3 – 0.7 µm) (Figure 10) is dominated by photosynthetic pigments with absorption maxima from 0.3 – 0.5 µm except for chlorophyll which has its absorption maxima at approximately 0.43 and 0.66 µm (chlorophyll a) and 0.455 and 0.64 µm (chlorophyll b) (Wessman, 1994). In the shortwave infrared (SWIR) (0.7-2.5 µm), vegetation has high reflectance in near infrared (NIR) from 0.7 – 1.3 µm and low reflectance in middle infrared (MIR) from 1.3 – 2.5 µm (Figure 10). The NIR plateau is influenced by cellular structure whereas the minor absorption bands occurring near 0.96 µm and 1.2 µm are a function of cellular arrangement and hydration state (Wessman, 1994). Leaf water absorption near 1.45 and 1.94 µm dominates in the MIR whereas cell structure, morphology and tissue constituents influence the intermediate region (Wessman, 1994).

The spectral variation of vegetation is complicated in natural vegetation due to the reflectance variability of the canopy. Studies by Asner (1998) have shown that standing litter is the most important factor for canopy surface reflectance variability, with the largest effects around 0.55 µm and 2.2 µm. According to Asner (*op cit*) the leaf area index (LAI) was the second most important factor causing a reflectance variability of 5% - 35% at roughly 0.72 µm whereas optical properties of green live foliage and percent vegetation cover played a small role in driving surface reflectance variability (3% - 11% and 1% - 2% respectively).

Possibilities and limitations

The deterministic approach i.e. direct identification of spectral objects in terms of spectral matching (see Section 1.1.3) is based on the absorption features in the spectral signal. In vegetation science the deterministic approach has therefore primarily been addressed within biochemistry. Spectral matching using continuum removed vegetation spectra has been used to map metal induced stressed vegetation (Collins et al., 1983; Singhroy and Kruse, 1991) and curve fitting has been used to model leaf water (Gao and Goetz, 1990).

Derivative spectrometry is an alternative method applicable to radiance data since the ratio of an any-order derivative of the at-sensor radiance at two wavelength approximately equals the ratio of the same order derivative of the spectral reflectance (Philpot, 1991). Derivative analysis of hyperspectral images has been used in mapping of both concentration and content of chlorophyll, nitrogen, lignin and cellulose (Curran et al., 1997). Derivative analysis is, however, sensitive to spectral smoothing. Hence, due to smoothing effects water content has been found to be more related to a simple ratio based on the relative depth of the water absorption feature at 1.156 µm than to correlation to first order derivatives at this wavelength (Rollin and Milton, 1998). A variation of the derivative analysis is based on characterisation of shifts in the chlorophyll absorption edge - the 'red-edge shift' (Wessman, 1994). The 'red-edge shift' is widely applied in agricultural sciences (see e.g. Broge et al., 1997).

Spectral mixture analysis in terms of full linear spectral unmixing or partial spectral unmixing are based on the assumptions that only linear mixing occurs. There are, however, several examples of the existence of residuals between linear mixing results and the original vegetation spectrum being unmixed. Several reasons for this have been suggested, e.g. the presence of non linear spectral mixing and incorrect choice or 'fuzziness' of endmembers (see e.g. Ray and Murray, 1996). Linear spectral mixture analysis has, nevertheless, shown that indicator variables of grassland management systems that reflect current structure and status of the system such as patchiness, leaf area index (LAI), biomass, soil and litter, can be extracted from hyperspectral image data (Wessman et al., 1997).

As the absorption features of vegetation are determined by the same few chemical components (Wessman, 1994) and as variation of vegetation structure and dynamics across plant communities imposes a large variability on the spectral signal (Graetz, 1990; Asner, 1998), identification of vegetation at a plant community level is complicated. The hyperspectral methods are based on the variation in absorption features between different targets of interest but due to the few and variable absorption features, the hyperspectral methods of spectral matching are not well suited for mapping of natural vegetation. Classification of plant communities has instead made use of hierarchical vegetation analysis and statistical methods optimised for class separation such as Canonical Discriminant Analysis mentioned in Section 1.3.1. Good results have been obtained with colour infrared aerial photography of high spatial resolution (Lobo et al., 1998) multi-spectral satellite data (Lewis, 1998) and hyperspectral data from the AVIRIS (Hoffbeck and Landgrebe, 1996).

24

1.4 Study area

The study area of this thesis was Mols Bjerge, Denmark, located on the peninsula of Djursland in the eastern part of Jutland (Figure 11). Mols Bjerge is one of Denmark's most hilly areas with a local relief between 0 and 137 m ASL. Mols Bjerge was formed during the last ice age 16,000 years ago when the area was located between two glacier tongues from the Young Baltic Ice Sheet. Accordingly, the area is characterised by terminal moraines pushed from both sides forming long, parallel ridges in the landscape (Larsen and Kronborg, 1994). Other dominant features are kames and kettles formed from a belt of dead ice behind the terminal moraines and deep erosion valleys formed by melt water.
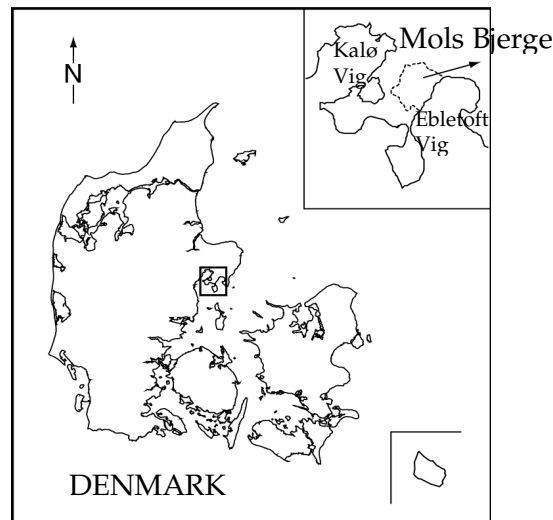
Figure 11: Denmark and the Mols Bjerge study area (inserted top right).

Cairns indicate that farming existed in Mols Bjerge already in the later Stone Age 6,000 – 5,000 years ago and many grave mounds indicate that the number of settlements increased in the early Bronze Age 3,000 – 2,500 years ago. From the Iron Age, 2,500 – 900 years ago the settlement was more permanent and relicts of this farming system are visible in the present landscape. Today, grasslands with occasional domestic livestock grazing replace the earlier cultivated areas and, apart from a few fields, open, dry grasslands, with naturally occurring shrub, thickets, deciduous forests and coniferous plantations dominate the area. On account of the glacial history of the area, which is clearly visible in the open landscape, its prehistoric remains and its rich flora and fauna, the northern part of Mols Bjerge was declared a protected area in 1977. The southern part was added to the protected area in 1992. The region covers approximately 20 square kilometres, of which about one third are vegetated by the semi-natural grasslands undertaken in this study (Figure 12). The high fragmentation related to physical distance or different management practices divides the grasslands into areas representing the full range of grasslands from old, unimproved grasslands with continuous grazing and high conservation priority to improved, sown grass swards still being part of a rotational farming system.

Figure 12: Photo of part of the study area, Mols Bjerge.

Semi-natural, dry grasslands are an important terrestrial Danish habitat as these areas support a large diversity of native plant and invertebrate species. Open grassland areas also act as corridors in the landscape for dispersion of flora and fauna species and only a minor part of Denmark is comprised by these semi-natural terrestrial habitats. Semi-natural terrestrial habitats have experienced a dramatic decline in the Danish landscape in recent years and large effort have been investigated in understanding these habitats.

1.5 Data collection/project set-up

Data for the whole project, including the pilot study, were collected over a four-year period from 1995 – 1998 during DANMAC (DANish Multisensor Airborne Campaign) campaigns. The project setup was extensive and covered the aspects described below. Of these aspects, this thesis focuses, as expressed by its objective (Section 1.1.3), on calibration of image data and image analysis for implication studies within grassland monitoring and mapping. The full data collection is described below.

1.5.1 Pilot study

Data for the pilot study were collected in 1995. The data for the study were collected for two old grassland areas with high and low plant species diversity and for two young grassland areas with high and low plant species diversity. Four plots (one for each grassland area) each consisting of one transect of six samples with 10 m interval were registered. Each sample consisted of 10 scans covering a sampling area of approximately 0.5 m². The data were collected from the 25 – 28 June 1995. The data were measured with GER (Geophysical Environmental Research) 2100 that operates in the region from 0.4 – 2.5 µm with a spectral resolution of 10 nm from 0.4 – 1.0 µm and 24 nm from 1.0 – 2.5 µm.

Statistical analysis showed that spectral discrimination of grassland age and in particular grassland plant species diversity was promising at the sample level in the VIS, NIR and mid-IR parts of the solar spectrum. Visual comparison of transect averages of the spectral signatures showed that old and young grasslands with different plant species diversities were less likely to be discriminated at the plot level probably due to the vegetation variation along the 60 m transects.

The pilot study was highly relevant as an indication of the prospects for the thesis study and the results were also the basis for the spectral and spatial configuration of the image data (Section 1.5.3) and the sampling strategy of the field mission in 1997 (Section 1.5.4). The work is not presented as part of the thesis, since the thesis, for the sake of coherence, covers the image analysis aspects of the study. Initial fieldwork before an airborne campaign is flown for identification of the potentials is, however, not to be underestimated and the pilot study has therefore been summarised here and included as the last article in Section 2.

1.5.2 Ecological data

In 1996 the study area Mols Bjerge was subjected to detailed ecological data collections by ecologists and botanists. All areas, excluding forest clearings, with more than 25% cover of grasses, forbs and dwarf shrubs, were identified and surveyed. 290 areas were assigned, in the field, to a management class and their plant species composition was registered.

Management map

Ecological parameters such as management history (age, grazing pattern, soil improvement), productivity and conservation interest (succession stage, plant species composition) were parameterised in relation to canopy variation detectable in the remote sensing signal and summed in a management map based on the following model considerations:

-) age determines the succession stage of grasslands, over time developing from highly productive areas to less productive areas. Age interpreted as variation in productivity (standing biomass) is a well-known biophysical parameter to be derived from remote sensing also from natural habitats (Tod et al., 1998);

-) soil improvement determines productivity;

-) cultivation determines species composition;

-) grazing determines vegetation composition of the grasslands, structure, dynamics and productivity. Structure and dynamics influence the remote sensing signal (Graetz, 1990). NDVI of grazed areas are better correlated to standing biomass than NDVI of ungrazed areas due to the presence, in the latter, of senescent and dry vegetation (Tod et al., 1998). The results suggest that the remote sensing signal is sensitive to grazing utilisation;

-) given that all other factors are equal (e.g. colonisation by new plant species), age, management (the sum of soil improvement and cultivation) and grazing determine the species composition.

On these ecological and remote sensing grounds seven grassland classes were defined and referred to as management (Ma) classes:

- old unimproved grasslands with continuous grazing (**Management class 1**),

- old, unimproved, previously cultivated grasslands (**Management class 2**),

- medium aged grassland, previously cultivated, but now with spontaneous dry grassland vegetation (**Management class 3**),

- young, formerly cultivated areas with spontaneous grazed vegetation (**Management class 4**),

- young, formerly cultivated areas with spontaneous ungrazed vegetation (**Management class 5**),

- 1 – 5 years old 'set-a-side' vegetation dominated by weed species (**Management class 6**), and

- improved, sown grass swards (**Management class 7**).

Ma classes 1, 2 and 3 were distinguished based on field assessment of long term land use history (> 250 years old with evidence of old farming systems), an index of indicator species for old grasslands of conservation interest (Ejrnæs and Bruun, 1995) and grazing patterns. Ma classes 4, 5 and 6 were distinguished on the basis of grazing patterns and field assessment of short-term land management. Topography, air photos (1945 – 1990) and landowner interviews supported the field assignment. A management map was produced from the field surveys with the assistance of infrared air photos acquired in 1995. For overview purposes this map (Figure 13) was digitised via feature duplication onto a digital image acquired with a GER 3715 scanner in 1995 (for data quality reasons these image data were not used in the thesis study).
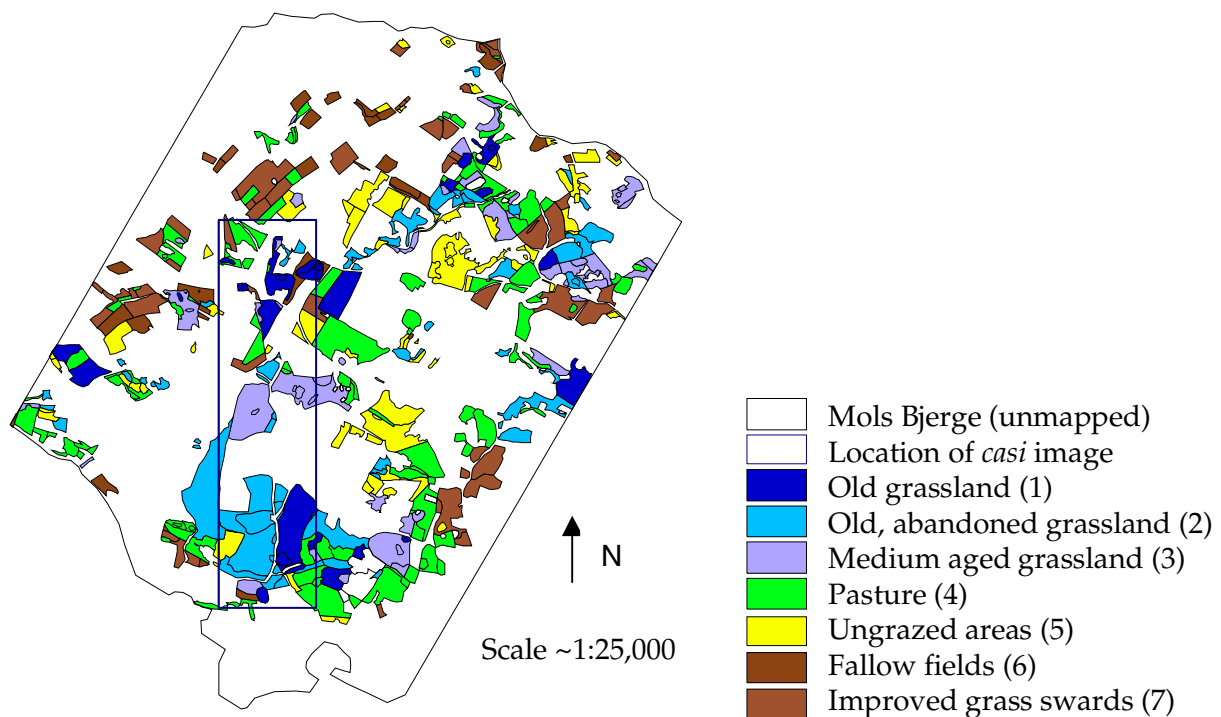
Figure 13: Management map of the seven management classes as field mapped in 1996 and location of the casi image.

The management map was used to plan the airborne mission, identify test sites for fieldwork during the mission and to interpret spectral classification of plant communities.

Plant species composition/floristic classes

Vascular plant species are often listed using an abundance scale (Kent and Coker, 1992). The abundance scale of this study was especially adapted to these large and often heterogeneous areas (Ejrnæs and Bruun, 1995). The abundance scale had four steps: 'present with low cover', 'frequent with moderate cover', 'frequent with high cover over at least part of the area' and 'high cover over the majority of the area'.

The vegetation data were combined with vegetation data from 30 test sites of 30 m by 30 m collected during the airborne mission in 1997 (Section 1.5.4) and subjected to floristic classification using gradient analysis and supervised clustering performed by a skilled ecologist (Jacobsen et al. 1999a and 2000b). The final model was used to predict the floristic

class (Fl class) for each of the grassland areas and the test sites, with Fl classes 1 to 7 relating to Ma classes 1 to 7 respectively (Table 2).

Class	Fl1	Fl2	Fl3	Fl4	Fl5	Fl6	Fl7
Ma1	6	8	7	1	0	0	0
Ma2	4	33	2	2	6	1	1
Ma3	4	7	16	6	3	0	0
Ma4	1	2	7	51	17	5	8
Ma5	0	7	3	18	36	6	1
Ma6	0	0	0	0	4	19	2
Ma7	0	0	0	3	0	2	34

Table 2: Combinations of management (Ma) and modelled vegetation affinity (Fl).

The management and floristic class assignments of the test sites were used in the spectral analysis of image derived apparent surface reflectance of the same test sites for spectral identification of plant species composition (Jacobsen et al., 1999a and 2000b) and are discussed further here.

1.5.3 Airborne data

The image data of the study were acquired with the *casi* scanner as the DANMAC project was multipurpose and the *casi* has the advantage of enabling specification of the spectral configuration for each individual flying mission.

Configuring the *casi*

The *casi* scanner (Figure 14) is a push broom linear array scanner with 512 sensors that operates in the spectral region from 0.4 – 0.9 µm.
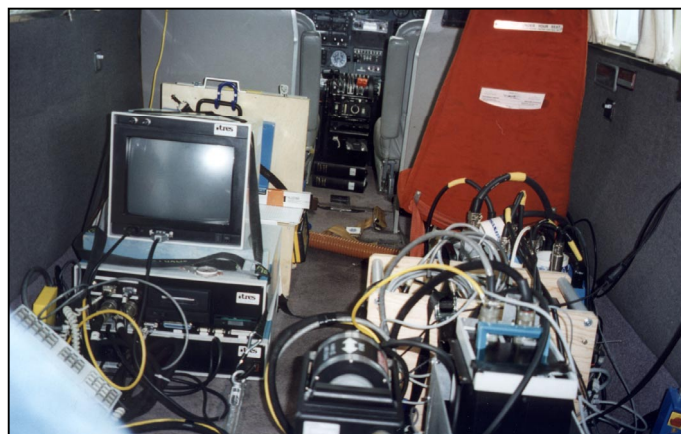
Figure 14: The casi scanner as installed in the aircraft for image acquisition.Photo: M. Stjernholm.

The *casi* operates in dual modes i.e. **i)** spectral mode, which acquires a contiguous spectrum in up to 288 bands with a spectral sampling of 1.8 nm for a varying number of pixels across track (39 to 512) and **ii)** spatial mode, which acquires up to 19 discrete bands for every 512 pixels across track. An incident light sensor (ILS) may also be deployed to measure the incident solar radiance during scanning. The particular scanner used in the study had a field

of view of 42° with, according to the operating company, a 5° discrepancy affecting the left most part of the view angle.

The configuration of the *casi* scanner used in the study was a trade off between spectral and spatial resolution. As a function of the IFOV of the scanner, the ground speed varies with the altitude of the aircraft under constant flying speed conditions. This means that the integration time of the scanner must be faster at higher spatial resolutions to obtain a complete coverage of the ground along the scan line. In spatial and spectral mode, reducing the number of bands reduces the integration time of the scanner. In spectral mode, reducing the number of look angles from the full 512 pixels across track down to 39 pixels also reduces integration time. The reduced number of columns may be recorded as adjacent columns along the nadir line or as discrete columns with pixel spacing across track to cover the whole swath.

The vegetation studies required high spatial resolution (Jacobsen et al., 1995) and data were scanned with a 2 m spatial resolution along the nadir line. This was considered adequate to spectrally identify individual trees and grassland vegetation since studies recommend 4 m² as a suitable sampling size for grassland vegetation community description (Økland, 1990). Given the *casi* integration time, eleven bands could be acquired at this ground speed. The spatial mode spectral configuration (KGRAS; Table 3) was developed with respect to Baulies and Ponts (1995) and the pilot study (Jacobsen et al., 1995).

Band	Min (µm)	Max (µm)	FWHM (nm)	Center (µm)
1	0.417	0.431	16.3	0.424
2	0.470	0.480	12.8	0.475
3	0.519	0.530	12.8	0.525
4	0.544	0.555	12.9	0.550
5	0.596	0.606	12.8	0.601
6	0.646	0.655	11.1	0.650
7	0.678	0.687	11.1	0.682
8	0.710	0.719	11.2	0.715
9	0.732	0.741	11.2	0.736
10	0.764	0.773	11.2	0.769
11	0.797	0.806	11.2	0.801

Table 3: KGRAS: 11 band spectral configuration of the spatial mode data used in the study.

Spectral mode data were acquired with the same spatial resolution as the spatial mode data. Priority was given to number of spectral bands over spatial coverage and 96 spectral bands were recorded for 39 look angles for every 9th pixel across track with approximately 5.4 nm spectral sampling in the region from 0.4 – 0.9 µm (Table 4).

Center wavelength (µm)	Center wavelength (µm)	Center wavelength (µm)	Center wavelength (µm)	Center wavelength (µm)	Center wavelength (µm)	Center wavelength (µm)	Center wavelength (µm)
0.394	0.458	0.522	0.586	0.650	0.714	0.779	0.844
0.400	0.463	0.527	0.591	0.655	0.720	0.784	0.850
0.405	0.469	0.532	0.596	0.661	0.725	0.790	0.855
0.410	0.474	0.538	0.602	0.666	0.730	0.795	0.861
0.416	0.479	0.543	0.607	0.671	0.735	0.801	0.866
0.421	0.484	0.548	0.612	0.677	0.741	0.806	0.872
0.426	0.490	0.554	0.618	0.682	0.747	0.812	0.877
0.431	0.495	0.559	0.623	0.687	0.752	0.817	0.882
0.437	0.500	0.564	0.628	0.693	0.757	0.822	0.888
0.442	0.506	0.570	0.634	0.698	0.763	0.828	0.893
0.447	0.511	0.575	0.639	0.703	0.768	0.833	0.899
0.453	0.516	0.580	0.644	0.709	0.774	0.839	0.904

Table 4: 96 band spectral configuration of the spectral mode data used in the study.

The *casi* mission

The mission was flown 10th June 1997, which was within the planned stand-by period of 2 weeks for image acquisition during the beginning of June. The pilot study had indicated good possibilities for spectral separation of grasslands during this period. This is the late spring season in this area, with the dead grasses from last year covered with fresh vegetation and, compared to the summer situation, when the burnt-off grasses are dominant, the vegetation is green and lush. Other studies have shown the major importance of this period for remote sensing of grassland vegetation (Turner et al., 1992). Earlier in the season, plant physiological processes associated with regrowth following defoliation influence the reflectance, whilst later in the season the accumulation of senescent material dominates the reflectance (Turner et al., *op cit*).

The flight campaign was implemented with a set of four pairwise parallel and perpendicular lines in spatial mode and a set of two perpendicular lines in spectral mode parallel to the spatial mode data (Figure 15). The two pairs of parallel flight lines (spatial data) were designed to each have an effective sidelap of 50%; this involved implementation with a 60% sidelap to account for the 5° extreme-left scanner discrepancy (Section 1.5.3). The two flight lines in spectral mode were planned to be overlapping a spatial mode flight line (Figure 15). However, these were actually flown in-between the parallel spatial mode flight lines.

One pair of the spatial mode flight lines and one spectral mode flight line were implemented almost due north (north 1° east) very close to solar noon to diminish bi-directional reflectance effects. This is because forward scattering of vegetation is stronger than backward scattering (Deering, 1989) – a problem that had been revealed in the airborne campaign in 1995 using the GER 3715 scanner data (Section 1.5.2). These data showed that the BRDF influenced the signal received by the sensor if the flight line were perpendicular to the direction of incident solar radiation. The flight lines were all flown under optimal weather conditions.

The flight line set-up of the mission was multi-purpose to cover **i)** data quality assessment; **ii)** developments of methods for application of hyperspectral remote sensing data within vegetation on semi-natural grasslands; **iii)** studies of bidirectional reflectance effects on

classification results dependent on illumination (flight direction) and view angle (position of the target across the scanline); and **iv)** eventual production of a full classification of grasslands in Mols Bjerge. Of these purposes, results relating to **i)** and **ii)** are presented in the thesis work. This work was performed on the north-south oriented scan lines K3 and K6, the data set that were flown almost due north. The data acquisition parameters of the two scan lines are shown in Table 5 and scan line K3 is shown in Figure 16.

Scan line	K3	K6
Orig Tape No.	3	3
Orig File	3	6
Date	10-Jun-97	10-Jun-97
Process	yes	yes
Heading	1 (N)	1 (N)
Start Time, Danish summertime	13:06:54	13:24:20
Local apparent time	11:47:30	12:04:52
Stop Time, Danish summer time	13:08:09	13:25:32
Integ Time(ms)	38	55
Time Dif (sec)	75	72
Scan Lines (Time dif/Integ time)	1974	1309
File size (x,y,z)	512, 2049, 11	40,1400,96
Byte order	Network (IEEE)	Network (IEEE)
Interleave	BIP	BIP
Pixel Width (m)	2	2
Pixel Length (m)	2	2.8
Configuration file	kgras	kgras / spec
No Bands or Looks	11	39
No row summation		3
No of Bytes	2.02E+07	1.11E+07
Center point E	10 32 04	10 32 15
Center point N	56 12 49	56 12 48
Roll correction	+	+

Table 5: Acquisition parameters of scan lines K3 and K6. BIP = Band Interleaved per Pixel.

Figure 15 (next page): The airborne flight mission as flown 10th June 1997. The map is reprinted with permission from the National Survey and Cadastre (G18/1997). (Layout Geoff Groom)

casi flightlines - Kalø-MolsBjerge

Base Map for this diagram :   UTM meters, Zone-32 :
KMS - 1:50.000

Flight line :	mode and spatial.res.	tilt-status	band-config.	line-up point : Easting	Northing	start-scan point : Easting	Northing	end-scan point : Easting	Northing
K-1	spatial - 2m.	nadir	KGRAS	589672	6230222	594117	6230222	597080	6230222
K-2	spatial - 2m.	nadir	KGRAS	601502	6229812	597061	6229812	594100	6229812
K-3	spatial - 2m.	nadir	KGRAS	595075	6224217	595075	6229274	595075	6232645
K-4	spatial - 2m.	nadir	KGRAS	595485	6224178	595485	6229265	595485	6232655
K-5	spectral - 2m.	nadir	KSPEC	601502	6229812	597061	6229812	594100	6229812
K-6	spectral - 2m.	nadir	KSPEC	595075	6224217	595075	6229274	595075	6232645
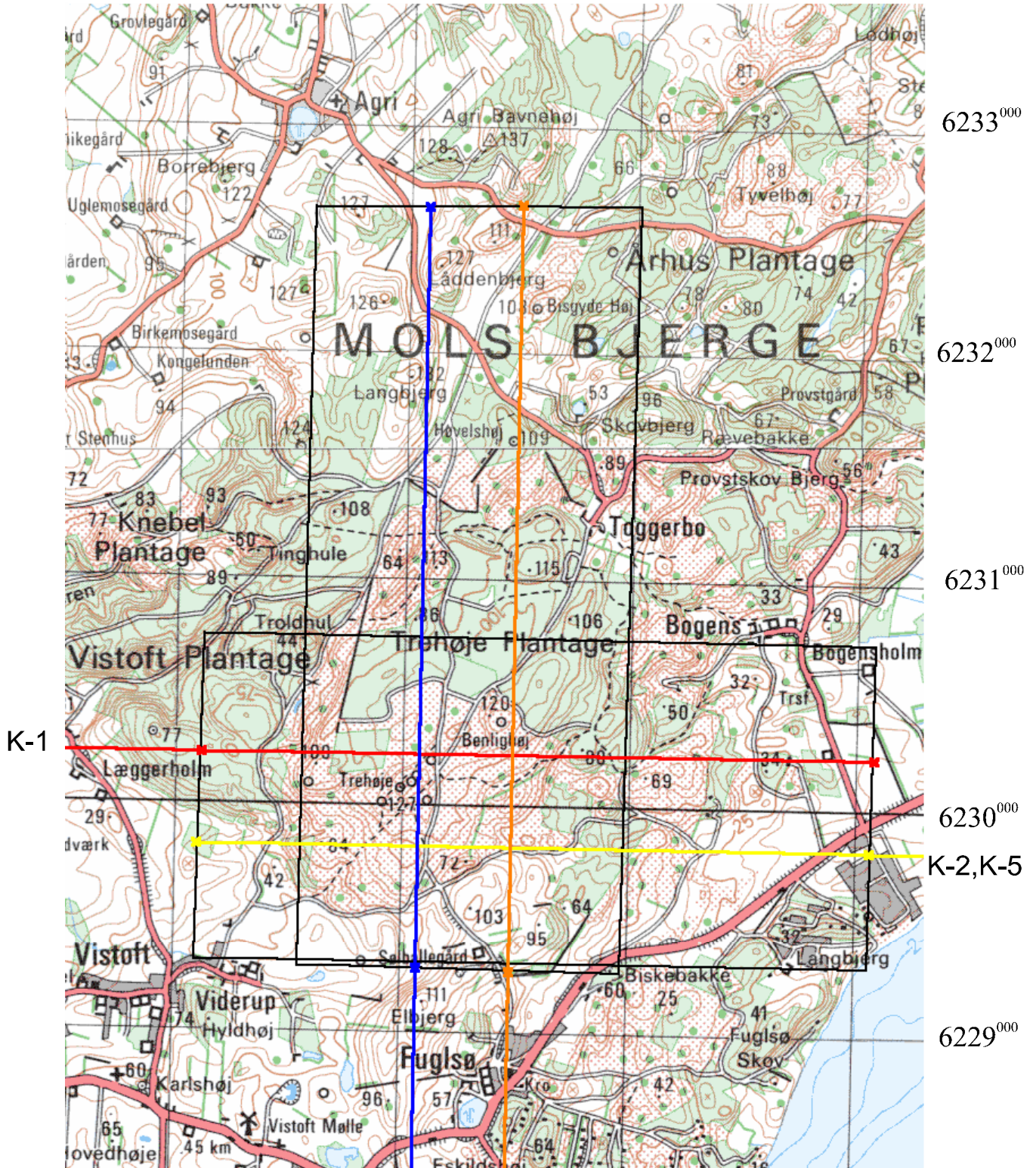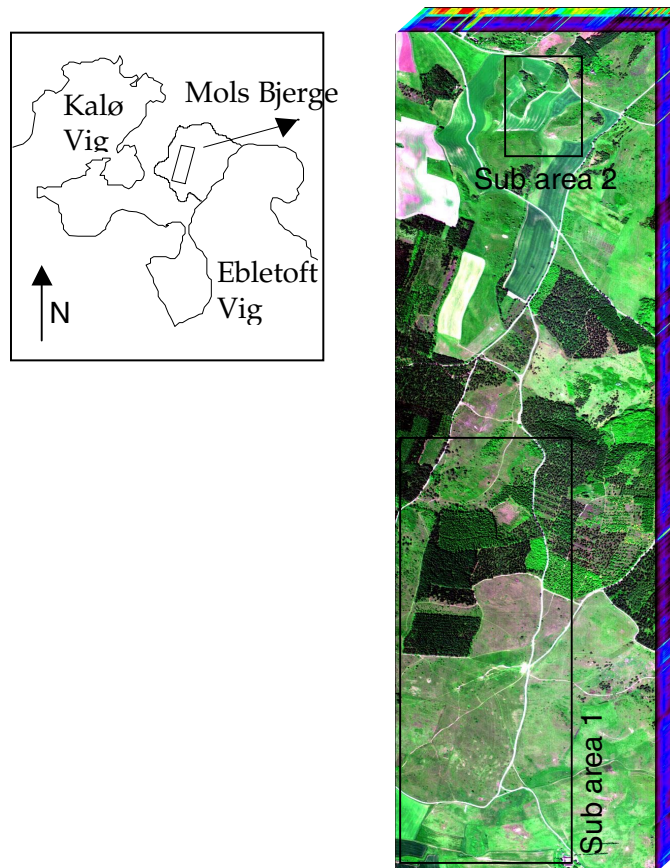
Figure 16: 3-d image cube of the spatial mode image data (K3). The colours on the edge faces represent the spectral radiance values for the edge pixels with 11 bands scaled 5 times. (r,g,b) = (682 nm, 650 nm, 475 nm). The two sub areas are investigated in the plant community mapping study. Approximate coverage: 1km by 3 km.

1.5.4 Field mission

Fieldwork (Table 6) was undertaken in connection with the *casi* campaign described in the preceding section. Based upon the management map, 30 test sites, comprising the seven management classes, were selected for ground data collection. The test sites were 30 m by 30 m as opposed to the 60 m transects of the pilot study (Section 1.5.1). The sides of each test site were oriented north-south (parallel/perpendicular to the flight lines) and the four corners of each were geopositioned in the field with an accuracy of +/- 2 m using Differential Global Positioning System (DGPS). The test sites were placed in level areas (16 out of 30) or in areas of constant slope and aspect that were considered to be as homogeneous as to be well described from one general plant species list. Plant species were registered within all test sites. The overall sampling strategy was different from that of the pilot study, which had shown that 10 m sampling was not valid to describe the spectral variation along a 60 m transect. A number of plot measurements i.e. point specific spectrometer measurements, plant species listing and biomass harvesting was also collected. The spectrometer measurements were performed primarily with the same GER 2100 instrument as in 1995 (Section 1.5.1).

Within the hilly Mols Bjerge area level sites of 30 m by 30 m, across a range of grassland classes, are widely dispersed, creating logistic problems for ground data collection simultaneous with an airborne mission. On the day of the *casi* overflights six of the 16 level test sites were chosen for selected ground spectrometry. At each of these six, a series of 90

randomly located spectral signature measurements were made, plus 25 randomly located plot measurements comprising point specific spectrometer measurements and plant species listing (Figure 17). Additionally, another thirty spectral signatures of a gravel parking lot were registered as a reference for atmospheric calibration of the image data.

Figure 17: Photo of fieldwork showing field botanist Torsten Krienke recording plant species in the target area of GER2100. Unfortunately, the analysis of these data is only preliminary and not presented in the thesis.

Within three days after the *casi* overflights, botanists completed a plant species registration for each of the 30 test sites. During this period too, 90 randomly located spectral signatures and a number of plot based spectrometer measurements and associated plot-based plant species listings were made at each of the remaining 10 level test sites. During the 10 days before and after the *casi* overflights point specific spectrometer measurements, together with species lists and biomass harvest were collected at three random plots within each of the 16 level test sites. A summary of the field mission is given in Table 6.

The field mission was planned as a follow-on to the 1995 pilot study of separation of grasslands with respect to age and plant species diversity, which had focused upon the important issue of field spectrometry. The 0.4 – 2.5 µm spectral signature measurements hold much information related to, for example, biochemistry and water stress. The purposes of collecting these data were to investigate **i)** whether the spectral configuration of the *casi* scanner was optimal for discrimination of grasslands and **ii)** whether important information for discrimination of grasslands lies beyond 0.4 – 0.9 µm, which is the spectral range of the *casi.* Another purpose of the field mission was development of a spectral library for mapping issues using spectral feature fitting algorithms (Figure 18).

Field data collected at the Kalø (Mols Bjerge) research site in 1997 in connection with optical remote sensing research.

'location' = homogenous 30 x 30 m areas representing 7 grassland classes
'plot' = small sample points within these locations

	Instrument or Method :	Comments :
day of CASI overflights (10 June)		**6 locations**
- location-based spectral signatures	GER-2100 or GER-2600	90 random measurements at each of 6 locations
- plot-based plant species list	botanists	25 random plots, at each of 6 locations (as above)
- plot-based spectral signatures	GER-2100 or GER-2600	25 random plots (same as above), 6 measurements per plot
day of CASI overflights		**gravel area**
- spectral signatures	GER-2100	30 random measurements
+ 3 days of CASI overflights		**16 locations**
- location-based plant species list		6 locations as above + 10 other
+ 10 days of CASI overflights		**the other 10 of the 16 locations**
- location-based spectral signatures	GER-2100 or GER-2600	90 random measurements at each location
- plot-based plant species listing	botanists	25 random plots, at each location
- plot-based spectral signatures	GER-2100 or GER-2600	25 random plots (same plots as above), 6 measurements per plot
+ / - 10 days of CASI overflights		**16 locations**
- plot-based spectral signatures	GER-2100 or GER-2600	3 random plots, at each location
- plot-based plant species list	botanists	GER-2100 plots : 10 x 20 cm; GER-2600 plots : 15,5 cm diameter
- plot-based biomass harvest	total above ground biomass	on the basis of the most dominant plant species present
-- fresh weight, dead & living matter	laboratory balance	on the basis of the most dominant plant species present
-- dry weight, dead & living matter	laboratory oven and balance	
At other times		**16 locations**
- UTM location (ED50 datum)	Trimble PathfinderPro Differential GPS	4 corner points (accuracy +/- 2 meters)

Table 6: Summary of field mission carried out in June 1997, in connection with the airborne casi mission (From: McCloy, 1997).
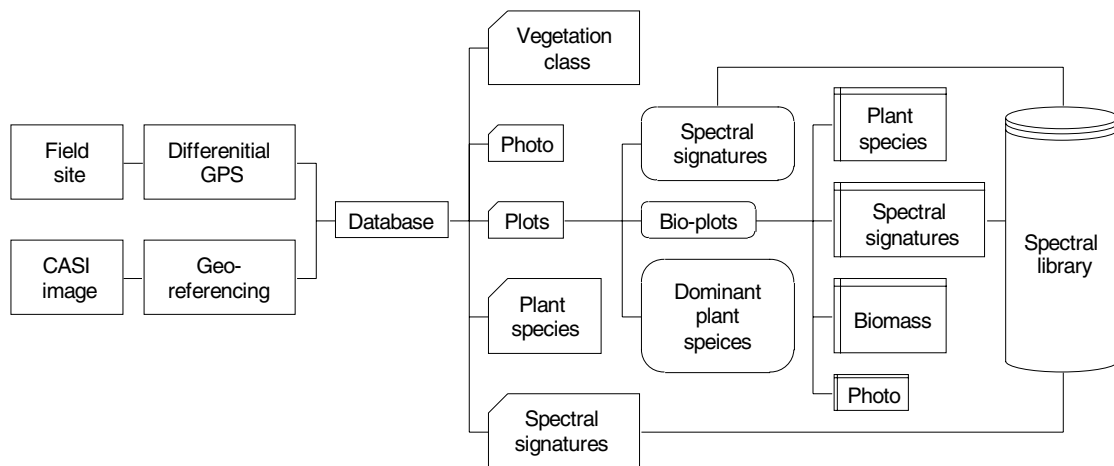
Figure 18: Spectral library diagram.

From the field work, the vegetation data of the 30 test sites were used for the floristic classification, and Ma, Fl, and MaFl class affinity and image derived reflectance spectra from the 18 test sites within the *casi* flight line K3 were used for spectral identification of vegetation composition (Jacobsen et al. 1999a and 2000b). The reflectance spectra of the gravel parking lot were used in the atmospheric calibration (Jacobsen et al., 2000a). Unfortunately, the field data of spectral measurements are not included in the thesis study due to the calibration of the spectral mode data (see Section 1.7.1).

1.5.5 Digital elevation data

During 1997 – 1998 a digital elevation model, based on topographical maps in the scale of 1:25,000 (2.5 m equidistant contours) updated in 1984 was developed (Figure 19). The DEM was available from 1999 and only used for georeferencing of the *casi* image to perform analysis of image spectra and, later, to perform analysis of classification results. The development of the DEM and georeferencing is presented in Jacobsen et al. (1999b).

1.5.6 Considerations

As mentioned in the introduction to this section, the data for the thesis study were collected over a four-year period. The data for the pilot study were collected in 1995 in the last half of June (Section 1.5.1). June was chosen for acquisition of the *casi* image data for plant physiological reasons and in order to use the experiences from the pilot study. Collection of ecological data of the Mols Bjerge study area was performed in 1996 (Section 1.5.2). This was a year before the *casi* campaign. The vegetation of semi-natural grasslands only changes slowly over time and it is therefore regarded acceptable that ecological fieldwork relating to plant species registrations was one year apart from the image acquisition. The image acquisition was in June 1997, two years after the pilot study. However, the ground data of the pilot study are not used with the 1997 *casi* data. Plant species recordings of the test sites used in this study were collected in 1997 within three days after the *casi* overflights, which is considered valid for the purpose. The field measurements of spectral reflectance were collected +/- 10 days of the *casi* overflights. In June, the changes in vegetation in terms of which plants that are in flower occur from day to day. It is given that these data, which may be measured up to 20 days apart, are influenced by this variation in time of measurement and therefore the field data may not be directly comparable to the image data. This means

that the value of the spectral library may be limited. On the other hand, it would be very difficult to collect as many data over a shorter period of time and, under the constraints given, it is probably difficult to obtain a better spectral library of semi-natural grasslands.
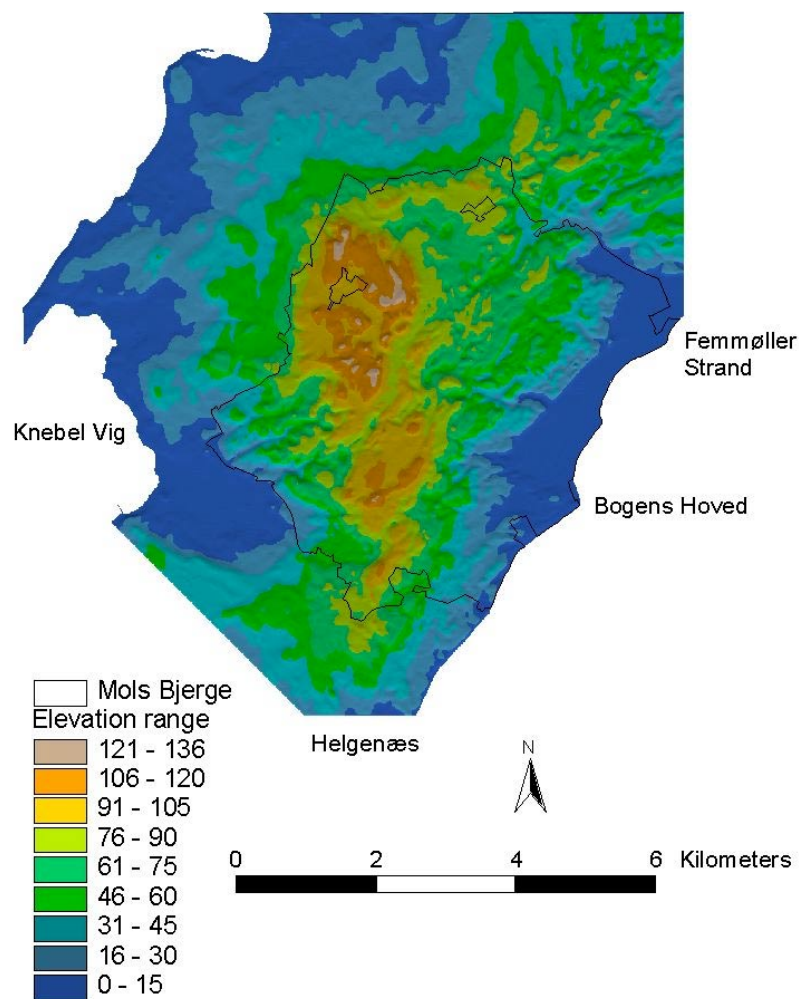
Mols Bjerge, Denmark

Figure 19: Digital elevation model of the Mols Bjerge area and surroundings.

1.6 Hyperspectral image analysis

The results of the hyperspectral image analysis including the data quality assessment, atmospheric calibration, image analysis, and georeferencing is documented in the five articles enclosed in Section 2. This section gives a brief summary of the methods, analysis and results, and conclusions.

1.6.1 Data quality assessment

The assessment of sensor calibration quality was performed to evaluate the image quality. This section is devoted to a summary of the quality assessment of the spectral and radiometric calibration of the *casi*. The article on which this summary is based in included in Section 2:

Assessing the Quality of the Radiometric and Spectral Calibration of CASI data and Retrieval of Surface Reflectance Factors by A. Jacobsen, K.B. Heidebrecht and A.F.H. Goetz. Photogrammetric Engineering and Remote Sensing, vol. 66, no. 9, pp. 1083-1091.

Radiometric calibration - summary

The data quality assessment in terms of the radiometric sensor calibration was based on the hypothesis advanced in Section 1.1.3 that the calibration quality could be assessed from the image data themselves and atmospheric modelling.

Method
We developed a method based on the theoretical concept that for a surface reflectance of zero, an airborne or spaceborne scanner will measure only path radiance and that the minimum signal in any band should equal at least the path radiance.

Analysis and results
The path radiance spectrum was modelled from MODTRAN (Berk et al., 1989) assuming zero surface reflectance and compared to a spectrum of the minimum radiance detected in each band in spectral mode. The minimum image radiance exceeded the modelled path radiance in several spectral regions since the minimum radiance was representative of a vegetated surface and not of a surface with zero reflectance (Figure 20). It was therefore expected that image minimum radiance exceeded path radiance around 0.55 µm (the green peak) and also from the red edge into the NIR region. It was, however, unexpected, and not obviously explained by biophysical principles, that the recorded radiance started to drop off significantly, relative to the modelled path radiance, below 0.448 µm, in several bands up to 0.467 µm and around 0.662 µm.

In the *casi* spatial mode data set the modelled path radiance was exceeded by the minimum recorded radiance in the first two bands at centre wavelengths 0.424 and 0.475 µm. This is an indication that the pattern extended beyond 0.467 µm. It was, however, only a few pixels that were effected in the second band. The problem was identified in bands 5, 6 and 7 at centre wavelengths 0.601, 0.650 and 0.682 µm, but less than 20 pixels were affected.. This is the region around the maximum chlorophyll absorption where reflected radiance is small and demands for radiometric sensitivity and calibration larger.
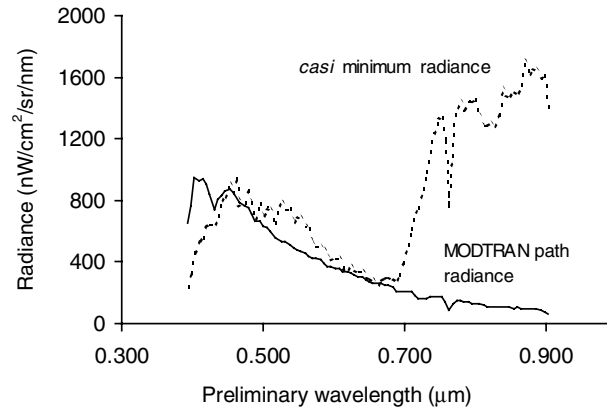
Figure 20: Path radiance spectrum and minimum radiance spectrum in spectral mode. Path radiance exceeds minimum recorded radiance in the shorter wavelengths and around the chlorophyll absorption feature.

The overall effect was interpreted as related to poor radiometric calibration of the sensor at shorter wavelengths and poor sensitivity in wavelengths in the regions with low radiance due to absorption from chlorophyll.

Conclusion
It was concluded from the results that the radiometric calibration quality could be assessed from the image data themselves by atmospheric modelling of the path radiance.

Spectral calibration - summary

The assessment of the spectral sensor calibration was based on the hypothesis (Section 1.1.3) that the spectral wavelength calibration of a high resolution continuously configured scanner and the precision of the spectral wavelength calibration can be obtained from modelling the centre wavelength of maximum absorption of narrow absorption features.

Method
We applied a method based on the concept that the narrow absorption feature of oxygen will provide a shift in modelled apparent surface reflectance around 0.782 μm unless the spectral calibration is accurate (Goetz and Heidebrecht, 1996). The spectral configuration was shifted until the reflectance shift was removed and the spectral wavelength calibration was obtained. The precision of the wavelength calibration was based on an oxygen fitting algorithm (Goetz et al, 1995, Goetz and Heidebrecht, 1996) and image statistics of an 'oxygen band centre' image – an image of the wavelengths with maximum oxygen absorption.

Analysis and results
Atmospheric modelling (Figure 21a) was performed using ATREM (CSES, 1997), scene specific parameters and a preliminary wavelength file. The spectral wavelength configuration was shifted 1/10 of a nm until a dominant shift near the oxygen absorption feature was removed (Figure 21b). The operating company finally confirmed the band centre position of the oxygen absorption feature at 0.7628 μm.
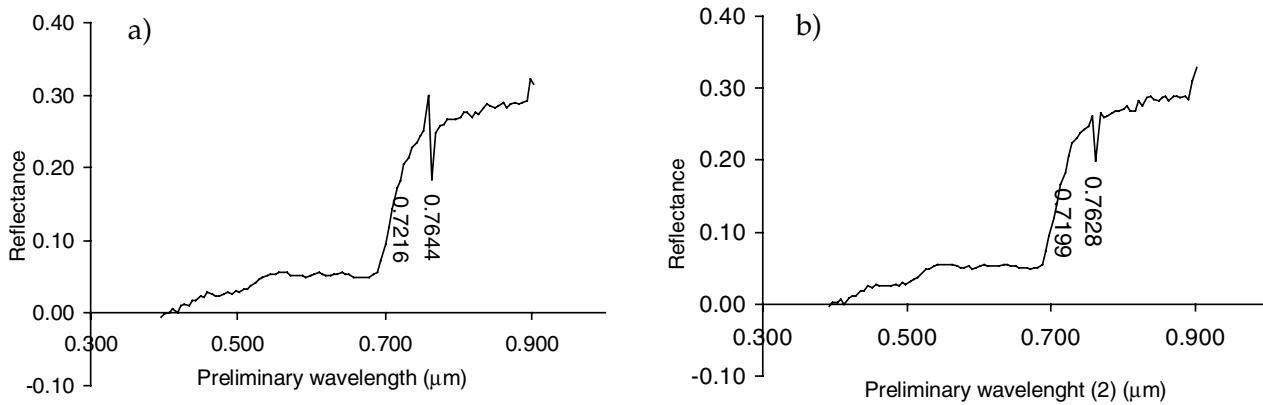
Figure 21: a) Apparent surface reflectance using a preliminary wavelength file. A spectral shift in the oxygen absorption is clearly seen in the data. b) Apparent surface reflectance after applying a constant shift to the preliminary band centre positions and, by doing so, creating new wavelength files until the shift in the oxygen absorption feature was removed.

It was clear from inspection of the image that the spectral calibration was inaccurate across the image and the oxygen fitting algorithm was applied. Statistics showed that the spectral precision along track was +/-0.25 nm (Figure 22a), whereas the spectral precision across track varied from +/-0.19 nm to +/-0.31 nm (Figure 22b). The along track standard deviation of +/-0.25 nm was exceeded by the 15 left most pixels of the image and the discrepancy was more than the 5° in the left part of the scanner as reported by the operating company.
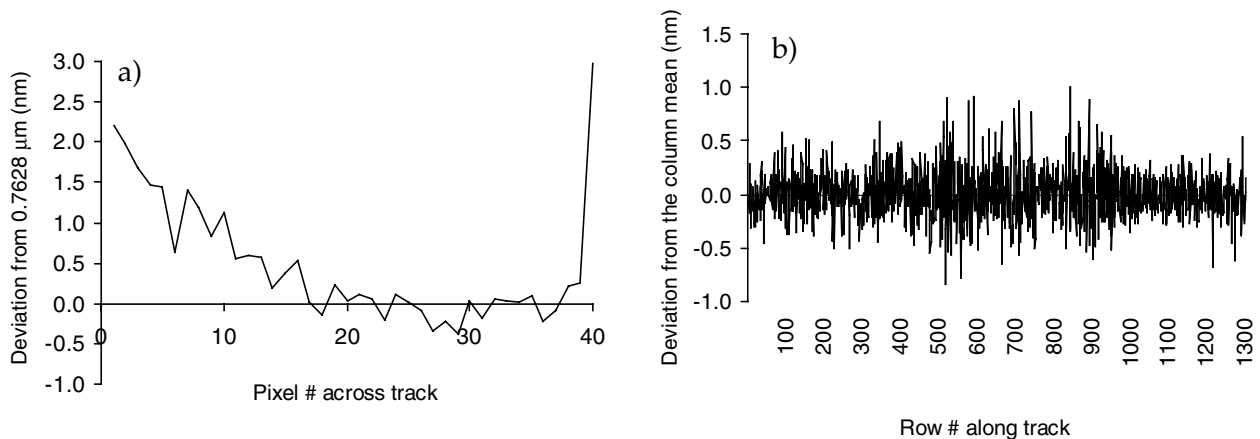
Figure 22: a) Horizontal profile across the oxygen image. Deviation in nm from 0.7628 μm. The spectral calibration precision clearly decreases towards the left part of the scanner and positive deviations up to 2 nm were found. b) Vertical profile across the oxygen image. Deviation in nm from the mean oxygen position of the column.

Conclusion
The results of the analysis proved that it is possible to obtain the absolute spectral wavelength calibration of a high resolution continuously configured scanner and the precision of the spectral calibration from modelling of the centre wavelength of maximum absorption of narrow absorption features, in this case oxygen.

43

1.6.2 Atmospheric calibration

This section is devoted to a summary of the atmospheric calibration of the spatial mode data. The summary is based on an article included in Section 2:

Assessing the Quality of the Radiometric and Spectral Calibration of *casi* Data and Retrieval of Surface Reflectance Factors by A. Jacobsen, K.B. Heidebrecht and A.F.H. Goetz. Photogrammetric Engineering and Remote Sensing, vol. 66, no. 9, pp. 1083-1091.

Summary

The atmospheric calibration of the spatial mode data was based on the postulated hypothesis (Section 1.1.3) that retrieval of surface reflectance factors can be achieved from a linear model based on one light calibration target and atmospheric modelling. The hypothesis was advanced as a consequence of the fieldwork that, due to the natural variation in the study area, only comprised one (light) calibration target.

The atmospheric calibration of the spectral mode data was based on atmospheric modelling and normalisation to field spectra. The method has not been put forward as a hypothesis since it is well-established (Clark et al., 1995; Goetz et al., 1997) and is not further discussed here since the data were not used in the image analysis due to the problems with spectral calibration (Section 1.6.1).

Method
The method developed for the spatial mode data was based on the concepts of the empirical line technique given that the gain describes the atmospheric transmission and the intercept describes primarily the path radiance (Goetz et al., 1997). A combination of these concepts and the principles of dark object subtraction, with the assumption that the only possible source of signal from a dark object is the path radiance, provided the background for the development of the linear model.

Analysis and results
The radiance from a surface with zero reflectance (path radiance) under the given atmospheric conditions was modelled using MODTRAN (Berk et al., 1989) and the path radiance profile was resampled to the spectral configuration of the spatial mode data. We used this value as the intercept and the ratio of at-sensor radiance and ground-based reference reflectance of a light target (a gravel - light coloured loose stone - parking lot) as the gain in the linear model.

A derived arbitrary vegetation spectrum and a field vegetation spectrum measured in the vicinity with the GER2100 were compared. Overall, the resemblance to a field spectrum was good. In the spatial mode data, the oxygen absorption feature in band 10 and the water vapour feature in band 8 were removed (Figure 23).
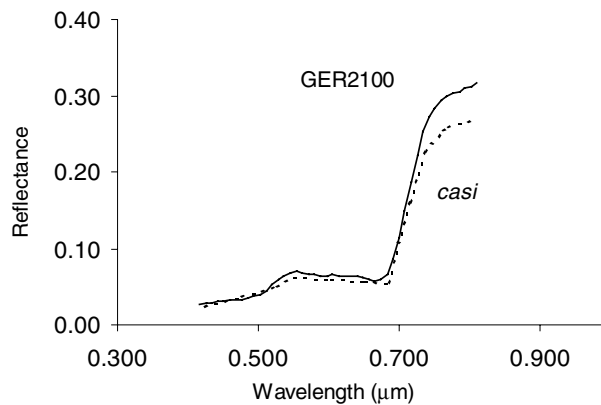
Figure 23: Derived vegetation reflectance spectrum (dotted) and field measured spectrum (solid) from the spatial mode image. There is a good resemblance between the two spectra. The difference in magnitude in the NIR is evident since the image pixel and field measurement locations were not identical.

Image statistics showed that negative reflectance occurred in bands 1, 2 and 5, 6, 7, which are the short wavelength region up to 0.475 μm and the region of maximum chlorophyll absorption. These results of the atmospheric calibration were similar to the result of the assessment of radiometric calibration, which was expected since both analyses were based on the same modelling of the path radiance profile.

Conclusion
It was concluded from the results of the spatial mode data that retrieval of surface reflectance factors can be achieved from a linear model based on one light calibration target.

1.6.3 Image analysis

The image analysis was divided in two subjects, one being encroachment as a matter of monitoring, the other being vegetation heterogeneity in terms of variation in plant species composition as a matter of mapping at a level suitable for research applications. This section is devoted to summaries of the implication studies. The articles that cover the subjects in full are included in Section 2:

Monitoring Grasslands using Convex Geometry and Partial Unmixing – a Case Study by A. Jacobsen, K.B. Heidebrecht and A.A. Nielsen. Schaepman, M., D. Schläpfer and K. Itten (eds.) (1998): 1st EARSeL Workshop on Imaging Spectroscopy, Remote Sensing Laboratories, University of Zurich, Switzerland, 6-8 October 1998, pp. 309-316.

Spectral Identification of Danish Grasslands Classes Related to Management and Plant Species Composition by A. Jacobsen, A.A. Nielsen, R. Ejrnæs and G.B. Groom. Proceedings of the Fourth International Remote Sensing Conference and Exhibition, 21-24 June 1999, Ottawa, Ontario, Canada, vol. I, pp. 74-81.

Spectral Identification of Plant Communities for Mapping of Semi-Natural Grasslands by A. Jacobsen, A.A. Nielsen, R. Ejrnæs and G.B. Groom. Canadian Journal of Remote Sensing vol. 26, no. 5, pp. 370-383.

Encroachment monitoring - summary

The study of encroachment monitoring was based on the hypothesis advanced (Section 1.1.3) that monitoring at the level of the individual is possible using spectral unmixing.

Method
We applied the automated extraction of endmembers proposed by Boardman (1995) taking advantage of the ecology of encroachment – slow advance of woody species at first few in number later increasing to smaller or larger coherent biotopes. The method applied included feature reduction using the MNF transformation, PPI and CEM.

Analysis and results
The analysis was performed on spatial mode data to insure full spatial coverage of the scene. The image had 135 columns of poor spectral calibration quality and two bands of poor radiometric quality excluded, leaving nine bands in the spectral region from 0.519 μm to 0.797 μm. The analysis was performed on MNF bands of apparent surface reflectance. Three PPIs were run. A rotating three-dimensional scatterplot of the purest pixels of the first run showed that agricultural fields were spectrally dominant. Excluding these areas and doing a second run showed that shade was spectrally dominant. Shade was excluded from the image using a CEM abundance map of 0.7 to 1.0 and the PPI was run a third time. Finally, two endmembers could be identified as deciduous forest (endmember 2) and coniferous forest (endmember 1).

The two endmembers mapped the two types of forest well, as well as individual large/old coniferous/deciduous trees. Generally speaking, trees at a late encroachment stage were identified but some areas of shade were also mapped as coniferous trees. Individual/coherent deciduous/coniferous scrubs (e.g. Juniper) were not mapped. Some areas of vegetated grassland were mapped as deciduous trees (Figure 25).

Conclusion
The results of the analysis showed that deciduous and coniferous forests were identified as endmembers and that individual woody species encroaching from the forests mapped well on derelict old grasslands where the individuals were old (large) or made a coherent surface cover. Scrubs and trees that did not originate from the forests were not identified as endmembers and were only mapped if they had a spectral signature similar to the forest species.
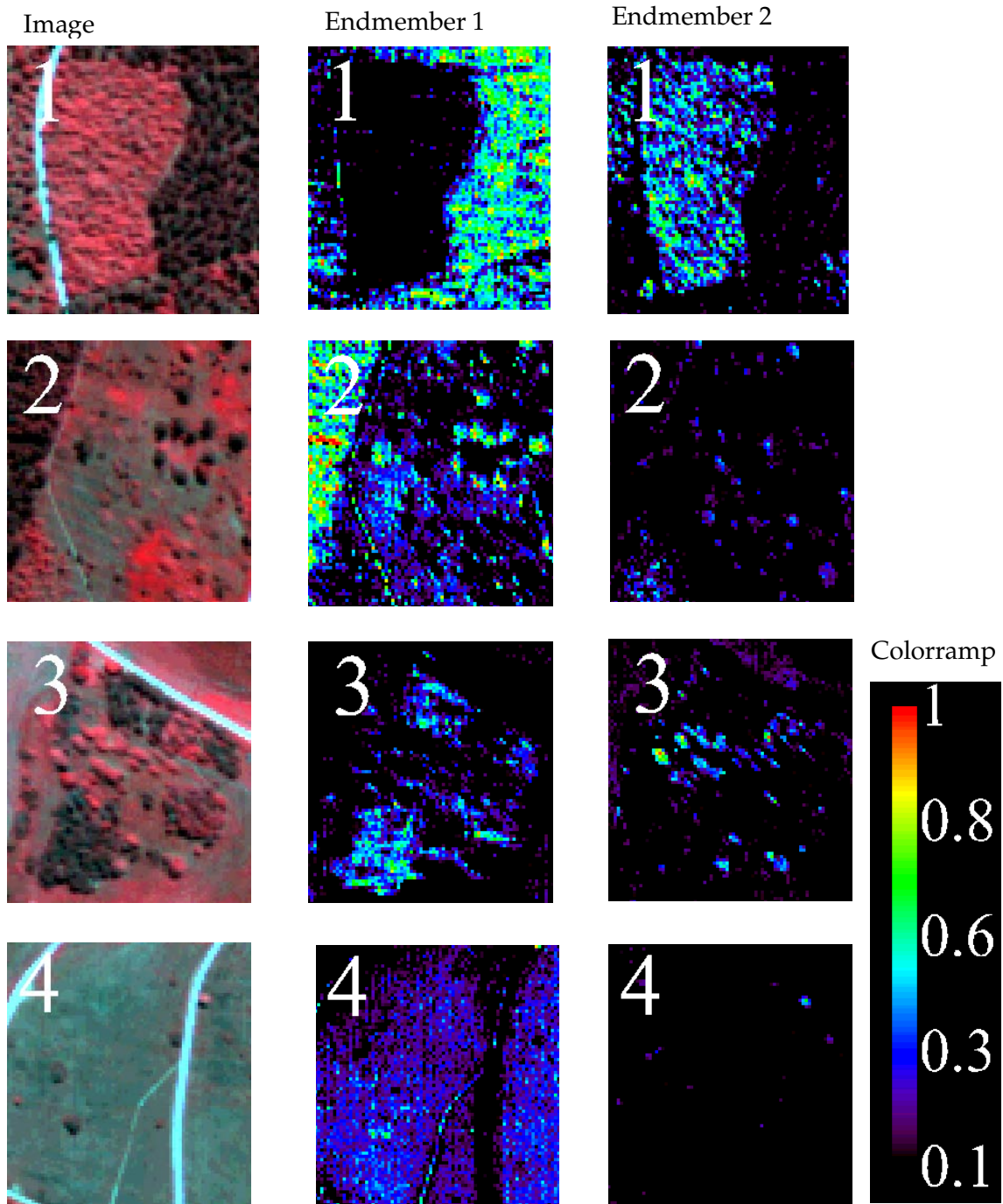
Figure 25: Four subsets of image K3 showing from left to right the original image (r,g,b) = (nir, red, blue), endmember 1 (coniferous forest) and endmember 2 (deciduous forest)

Mapping of vegetation heterogeneity - summary

The mapping of vegetation heterogeneity was based on the hypothesis advanced (Section 1.1.3) that the source of spectral variation of vegetation within areas of the same management category is related to plant species composition.

Method
We developed a method based on **i)** the ecological and remote sensing aspects of age, management and grazing (Section 1.5.2) and **ii)** the statistical concept that good training classes should be unimodal and well-separable. A hierarchical approach first divided a number of test sites into management classes (Ma classes) reflecting canopy variation (structure, dynamics and productivity) determined by soil improvement and cultivation. Secondly, these management classes were divided until they were spectrally unimodal. The method was evaluated with separability measures and the results of the gradient analysis and the floristic clustering of the species data. The method spectrally identified test site classes related to management and floristic – the MaFl classes. The MaFl classes were grown into training classes and a maximum likelihood classification was performed. The confusion matrix was thereafter evaluated with respect to the floristic variation as described from the gradient analysis and the floristic clustering.

Analysis and results
The analysis was performed on 18 test sites within the *casi* image unaffected by poor spectral calibration quality using surface reflectance data of nine bands in the spectral region from 0.519 µm to 0.797 µm. CDA was performed to evaluate spectral consistency of test site classes using artificial clustering within the test site groupings; the J-M distance was used to measure pair-wise spectral separability. The spectral separability between classes was improved from Fl classes to Ma classes to MaFl classes to seed-grown MaFl classes. In general terms, the spectral analysis and the confusion matrix of the maximum likelihood classification proved that the spectral variation within Ma classes could be explained by floristic variation. The result of the maximum likelihood classification is shown in Figure 26.

Conclusion
The results indicated that the source of spectral variation of vegetation within areas of the same management categories might be related to plant species composition and that spectral mapping of vegetation heterogeneity related to plant communities may be performed with hyperspectral data.

Maximum likelihood classification results of spectral MaFl classes

Ground based management areas with the same MaFl combination as the spectral MaFl classes
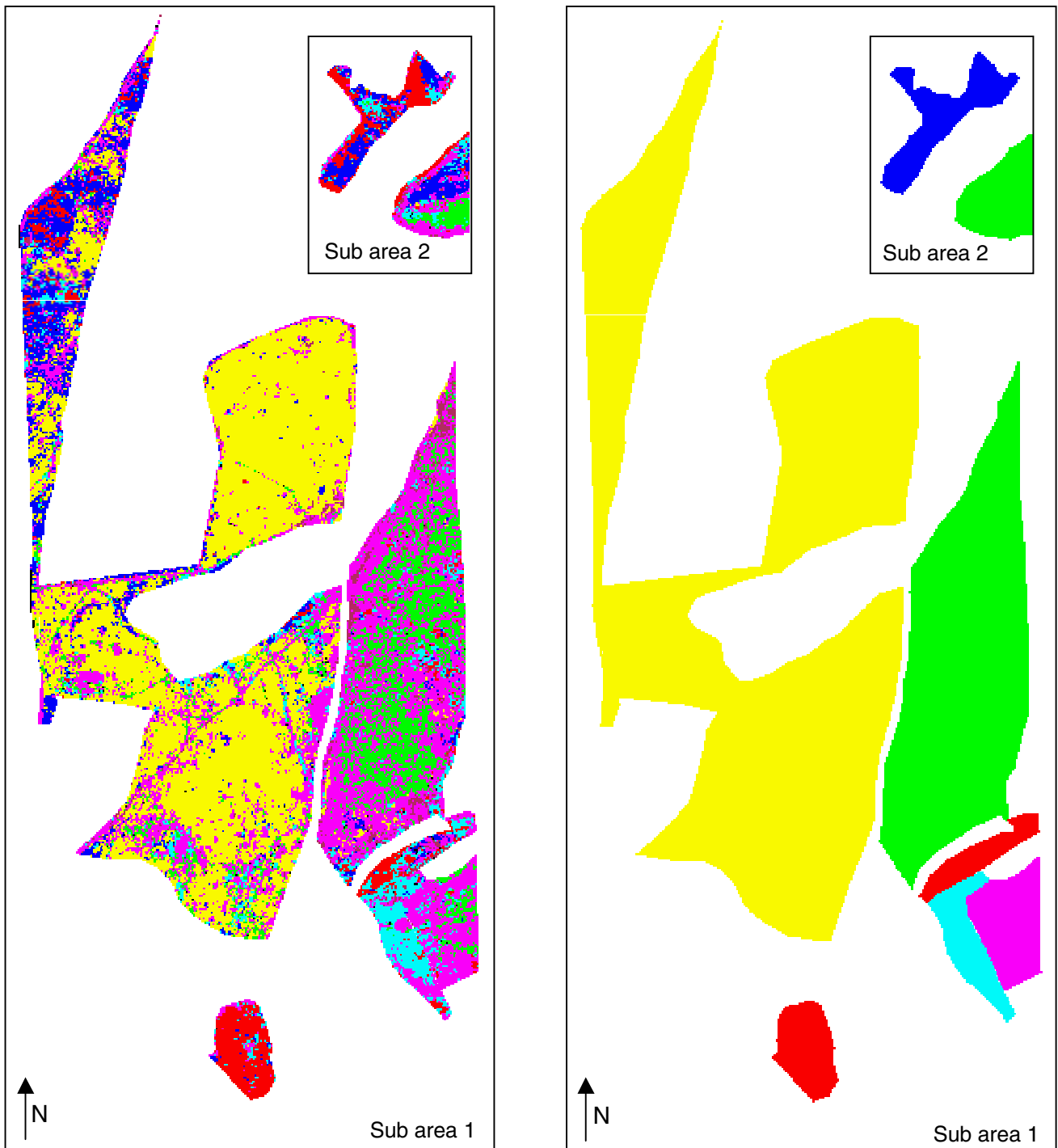
Legend:

Red:	MaFl 1.1	Blue:	MaFl 2.1	Purple:	MaFl 3.3
Green:	MaFl 1.2	Yellow:	MaFl 2.2	Cyan:	MaFl 5.5

Figure 26: Maximum likelihood classification of six MaFl classes (left) and management map (right). The location of sub areas 1 and 2(inserted top right) are shown in Figure 15.

1.6.4 Georeferencing

This section is devoted to a summary based on the results achieved and presented in an article in Section 2:

Generation of a Digital Elevation Model of Mols Bjerge, Denmark, and Georeferencing of Airborne Scanner Data by A. Jacobsen, N. Drewes, M. Stjernholm and T. Balstrøm. Danish Journal of Geography, vol. 99, pp. 35-46.

Summary

The georeferencing was based on the hypothesis advanced (Section 1.1.3) that automated extraction of an unlimited number of terrain tie points from a high resolution digital elevation model and TIN (Triangulated Irregular Network) resampling can be used to correct for terrain effects induced by platform attitude variations.

Method
The method was based on the concept that modelling, incorporating corrections for panoramic and topographic effects, of a waste number of terrain tie points to image space prior to piecewise TIN warping would account for the topographic and panoramic distortions in the image as well as the attitude induced distortions. The method developed used piecewise triangle warping (TIN resampling) based on GCPs supplemented by iteratively interpolated new tie points found by triangulation in both map and image space (Devereux et al., 1990).

Analysis and results
A grid based digital elevation model (DEM) was the basis for development of a DEM in TIN form. The approach was an iterative Delaunay triangulation of vertices based on a initial set of 65 ground control points (GCPs) interpolated to a TIN DEM. Each initial triangle was tested to see whether the difference between the regular grid DEM and the TIN interpolated DEM was above an acceptance level of 1m. If the difference exceeded the acceptable level, a new vertex was added to the positions where the maximum divergence in both the positive and negative directions was detected and a new TIN DEM was interpolated. The process was repeated until the acceptance level was reached which resulted in 6500 vertices to describe the terrain.

Based on the 65 GCPs, the image coordinates of the 6500 tie points were automatically extracted, including correction for panoramic and topographic distortion, and the image was warped using TIN resampling. The TIN resampling was compared to nearest neighbour resampling, corrected for topography and panorama, based on polynomial distortion models of the initial 65 GCPs, corrected for topography and panorama, and gravel roads and foot paths in the area tracked with DGPS and superimposed on the image.

Delaunay triangulation including iteratively extracted vertices from a grid based DEM turned out to be substantially important for the overall georeferencing accuracy. Comparison between the resampled images using 3rd order polynomial modelling and triangulation proved that georeferencing was especially improved in off-nadir hilly areas that lacked GCPs (Figure 27). In these areas closeness in correspondence between the tracked paths and the TIN resampling was found and inclusion of vertices extracted from the DEM had corrected for terrain as well as attitude variations.
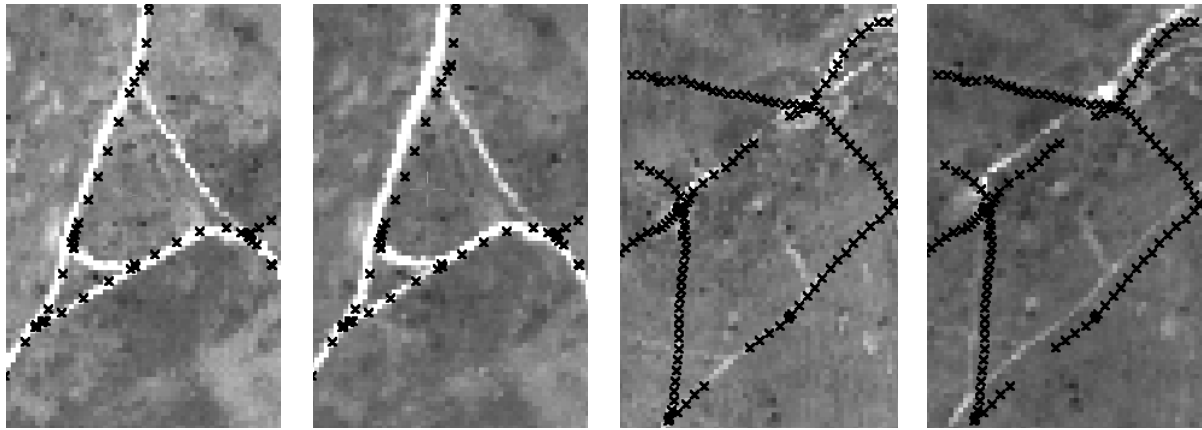
Figure 27. Four subset showing the results of triangulation (first and third image from the left) and 3rd order polynomial distortion modelling (second and fourth image from the left). Subsets 1 and 2 from the left are a region along the nadir line; subsets 3 and 4 from the left are an off-nadir hilly area.

Conclusion

It was concluded that automated extraction of an unlimited number of terrain tie points from a high resolution digital elevation model and TIN resampling could be used to correct for attitude induced terrain effects.

1.7 Discussion of results and research methods

The summaries in Section 1.6 are based on the relevant articles covering the five hypotheses stated in Section 1.1.3 presenting a range of issues within airborne hyperspectral remote sensing and its implications for monitoring and mapping of semi-natural grasslands. In this section evaluation is made of the approaches used in the articles, based on the theoretical concepts presented in Sections 1.2 and 1.3. The evaluation follows the headings of the three step process of hyperspectral image analysis introduced in the beginning of the thesis (Section 1.1.2), namely, **i)** calibration of image data, **ii)** development of methods for image analysis, and **iii)** georeferencing of the end product.

1.7.1 Calibration of image data

It is established in Section 1.2 that calibration of image data to apparent surface reflectance is a process of importance to ensure that image analysis is based on the target reflectance properties and not the reflectance, absorption and emission properties of the atmosphere. Atmospheric calibration is thus of importance to any image analysis, with increasing importance if the image data are analysed with ground spectra or if bi- or multi-image (-temporal) analysis is performed. It is also given that successful retrieval of apparent surface reflectance is reliant on well-calibrated data.

As a result of these considerations, it was decided to perform the image analysis for the implication studies on image data reduced to apparent surface reflectance. The data quality of both *casi* modes and the spectral wavelength calibration of the spectral mode data were assessed and the data were calibrated to apparent surface reflectance (Jacobsen et al., 2000a). The assessment was based on the hypothesis given in Section 1.1. The method, analysis and results, and conclusion were summarised in Sections 1.6 and 1.7.

Image Quality

For assessment of the quality of the radiometric calibration we developed a method that applied modelling of the path radiance and retrieval of an image radiance spectrum of the minimum radiance detected in each band. Minimum radiance was lower than path radiance below 0.467 μm and around 0.662 μm in the spectral mode. Minimum radiance was lower than path radiance in bands 1 and 2 (centre wavelengths 0.424 and 0.475 μm) and, for a few pixels, in bands 5, 6 and 7 (centre wavelengths 0.601, 0.650 and 0.682 μm) in the spatial mode data.

It was concluded in Jacobsen et al. (2000a) that the reason for the low signal was poor radiometric calibration at shorter wavelengths and around the chlorophyll absorption feature. A point that was not made in Jacobsen et al. (2000a) was that the effect is also likely to be a matter of sensor sensitivity rather than spectral resolution. The sensor sensitivity of the *casi* decreases towards the extreme ends of the spectral region (*casi* Training Manual, 1995). Hence, it may be that the spectral bands in the spatial mode data were configured too narrow to match the radiometric sensitivity of the sensors even though the bands in the shorter wavelengths were configured broader than the other bands (Table 3). Others have chosen an even broader band resolution of around 30 nm below 500 nm (Baulies and Pons, 1995; Blackburn and Milton, 1997). The same effect was seen in both the spatial and the spectral mode data. Therefore, it is considered likely that it is a matter of either poorly

calibrated detectors or, if indeed it is a matter of sensitivity, that this *casi* scanner had a true spectral range much narrower than indicated in the specifications.

For assessment of the spectral calibration we developed a method applying modelling of the oxygen absorption feature and retrieval of surface reflectance factors. The method was applied to the spectral mode data. We identified an absolute spectral wavelength calibration that was later acknowledged by the operating company. The oxygen absorption modelling also revealed that the spectral alignment problems influenced a larger part of the scanner than specified by the operating company. We identified a mean spectral calibration inaccuracy of 0.25 nm across track, resulting in exclusion of 15 columns most affected by the discrepancy. The method for assessment of spectral calibration accuracy could not be applied to the spatial mode of discrete bands. At the time (Jacobsen et al., 2000a), a method for assessing this data set was not developed. Instead, it was merely assumed that since 15 columns in spectral mode were equivalent to 135 columns in spatial mode, 135 columns would be likely to be affected in spatial mode.

It was concluded that at a 5.4 nm sampling, the accuracy of the spectral calibration must be better than 0.25 nm to account for the sharp oxygen absorption feature at 0.762 µm. Goetz et al. (1991) found that in the water vapour absorption regions from 0.7 to 2.3 µm an accuracy of 0.1 nm was desirable at a 10 nm sampling interval as 10 nm resampling is narrow compared to the water vapour features. In general, the demand for spectral accuracy is a function of the relationship between the width of the absorption feature and the spectral resampling. The results of the data quality assessment of the spectral mode image data led to a rejection of these data for further analysis. The atmospheric calibration of the spectral mode data is therefore not presented in the summary section and hence not discussed in this section.

Other approaches for assessing quality of data from a linear array scanner includes transformation of data to MNF feature space (Larsen et al., 1998; Nielsen and Larsen, 1994). An MNF transformation of the spatial mode data including all 512 columns was performed as part of the analysis in Jacobsen (1998) (not presented as part of this thesis). The MNF transformation actually revealed that 135 columns were affected by the discrepancy (seen as a darker area in MNF band 3). The MNF transformation also detected bad performance of two detectors seen as two bad columns along the image (Jacobsen, 1998). These two adjacent bad columns were substituted with the average of the two adjacent columns since the columns pixels were so spectrally significant that they were the covariance drivers of the image and accordingly identified as target endmembers in a PPI process. The radiometric calibration problem was not detected in the MNF images. The spectral mode data were a resampled image of every 9th pixel across track and the noise estimation performed as a 'shift difference' (BSC, 1997) hence MNF transformation could not have performed successfully on this data set.

The MNF method gives the option of removing the noise and restoring the original bands but it cannot supply information of calibration accuracy in absolute units as can the method developed in this study. Harron et al. (1992) used a standard lamp and diffusing panel and an integrating sphere to assess the absolute and relative calibration of a *casi* scanner. These methods gave a range of information on the systematic and random errors in the calibration of a *casi* scanner. The methods were dependent on accessibility of the scanner and laboratory facilities. The information given by the method used in this study was simpler and less detailed but also cost-efficient and ready-to-use in its approach of relying on the image data themselves in the evaluation process.

Atmospheric calibration of spatial mode data

The atmospheric calibration of the spatial mode data was performed as a normalisation of the image spectra by first subtracting the path radiance and second applying a gain based on the ratio between image and ground reference spectra. By these means, the derived apparent surface reflectance assembled field spectra and the oxygen absorption feature and the water vapour feature were removed.

The method was a linear model applied to all pixels in the image. As such the differences between pixels were unchanged since no pixel-to-pixel calibration was performed (Gao et al., 1993). It ensured that image analysis was performed on spectra that was not influenced of the atmospheric effects seen in the data such as oxygen absorption.

The combination of atmospheric modelling and normalisation to reference spectra is a well-known and recommended technique in atmospheric calibration of hyperspectral data (Clark et al., 1995; Goetz et al., 1997). The established methods rely on atmospheric modelling of apparent surface reflectance followed by normalisation to ground spectra - as performed on the spectral mode data (Jacobsen et al., 2000a) but not further discussed here. The approach used to retrieve apparent surface reflectance of the spatial mode data is different in that it models the path radiance and uses this as the intercept in an empirical line type of approach. The approach has the benefit of limiting the number of reference targets to one light-coloured target, which may be beneficial if no natural reference areas are present in the study area.

1.7.2 Image analysis

The methods developed for image analysis were related to implications for the monitoring and mapping of semi-natural grasslands. The methods were developed from the basic ideas of hyperspectral work relying on extraction of information based on variation of spectral reflectance in the image. It has been discussed (Section 1.3) that valid methods include reduction of data dimensionality to a feature space describing the spectral dimensionality in the image using fewer (decorrelated) bands that are related to the signal alone. Accordingly, the approaches used here have been based upon this technique. The section is a discussion of the developed methods of research relevant to the hypotheses within this topic as given in Section 1.1 and the summaries given in Section 1.6.3.

The monitoring and mapping of grasslands were divided into two parts: **i)** Encroachment of woody species onto grassland and **ii)** spectral identification of plant communities and subsequent mapping. The methods applied and developed (Jacobsen et al., 1998, 1999a, 2000b) took into consideration the special character of the targets to be mapped and the effect of structure and dynamics on the spectral signature of canopies of different species composition.

The implication studies were performed on surface reflectance on a subset of nine bands, with the exclusion of 135 columns. If this had not been so, the spectral mis-alignment would have influenced the difference between pixels and thus the spectral analysis and mapping results. The poor radiometric calibration of spectral bands 1 and 2 did not influence the difference between pixels but these bands were excluded since the mutual dependency between pixels was less reliable due to the insensitivity/poor calibration of the sensors.

Partial spectral unmixing for encroachment monitoring

For encroachment monitoring, the method of Boardman (1995) was applied, including transformation to MNF feature space, PPI analysis and partial spectral unmixing using CEM. Three endmembers were found and interpreted as shade, deciduous and coniferous forests and partial unmixing was performed of the latter two. Woody species encroaching from the forests were mapped on derelict old grasslands where the species were old (large) or made a coherent surface cover. Trees and areas of scrubs that did not originate from the forests were only mapped if they had a spectral signature similar to the forest species. Some areas with shade came out as coniferous trees and only a few individual bushes and trees out in the open grassland areas were mapped.

It has been possible to find only one other vegetation study that has used CEM for mapping of vegetation. Farrand and Harsanyi (1994) used CEM for mapping of green vegetation in a sparsely vegetated area in an AVIRIS scene and recommended it for its ability to minimize the background materials and enhance the green vegetation. Full spectral unmixing have been more widely applied in vegetation studies (Gamon et al. 1993, Wessman et al., 1997) but this was not an option in the present case since we were interested in only a few out of several potential endmembers. Vegetation studies have not been found that use partial or full spectral unmixing for identification of vegetation based on their spectral signature such as occurs in geological science. This is probably because vegetation is made up of the same chemical constituents, which imposes the same shape to any vegetation spectrum (Wessman, 1994) and since canopy reflectance is obscured by variability in litter and LAI which has a large impact on the spectral signature (Asner, 1998).

CEM was applied in this study based upon the ecology of encroachment and visual inspection of the image data. It appeared that woody species covered only a few pixels in the grassland areas and that they were visually distinguishable from the background grassland reflectance. It was therefore decided to focus on a method that **i)** had been developed explicitly to identify targets that are few in number and spectrally unique from the background reflectance and **ii)** could perform at a sub-pixel level since it was considered that individual species would have a spatial coverage of less than 2 m squared - the ground resolution of the *casi* image. Automated extraction of endmembers was applied (PPI), followed by partial spectral unmixing. The design criterion was that woody species were not only few in number but also as spectrally significant as to be identified as endmembers in a convex geometry process and the success was dependent on this.

The intention was to use a mask of the grassland areas based on the management map in order to perform the analysis on these data. Unfortunately this was not an option since, at the time, the management map and the *casi* image was not co-registered and the analysis was performed on the whole image. This meant that the individual scrub species and trees did not have a sufficient number or a significant spectral signature to be identified as endmembers. This puts a limit to the monitoring of the general encroachment stage on grasslands using this method but, on the other hand, the abundance maps of the forest species may become an important source for assessing the importance of biotope references to encroachment on derelict grasslands.

CDA and ML classification and mapping of plant communities

The task of this study was to design the right criteria for a spectral analysis to investigate if spectral differentiation of vegetation variation within natural vegetation, of merely the same structure and at the same phenological stage, was possible with airborne hyperspectral data. The basic concept was to build a bridge between spectral and vegetation data by developing a hierarchical approach that took into consideration the reflectance characteristics of vegetation.

Due to the variability of vegetation reflectance as a function of structure and dynamics (Graetz, 1990; Asner, 1998) a hierarchical approach was developed that divided a set of test sites into first management classes (Ma classes), based on ground-based information, and second floristic classes (Fl classes), based on modelling. On these grounds, it was possible to identify management related plant community classes (MaFl classes) spectrally. Lobo et al. (1998) performed a very detailed study of colour infrared image data separated into three spectral bands and from image segmentation and CDA they identified four land cover classes across the segments: bunch grasses, dense annual grasses, sparse annual grasses and bare ground. In the thesis study, 11 MaFl classes were identified using nine bands.

CDA was used to investigate if the hierarchical approach was spectrally and statistically valid for identification of plant communities in terms of their being well-defined and well-separable. Gradient analysis (DCA) was used to evaluate the spectral clusters floristically. The identification of training classes related to plant communities was followed by a maximum likelihood (ML) classification since the spectral analysis was ensuring that the training classes were unimodal and well-separable. Seed growing was performed before classification to ensure proper estimation of the covariance matrix. ML classification of the image and its superimposition on the management map added detailed information on vegetation heterogeneity by interpretation of the confusion matrix and the vegetation ordination diagram based on DCA.

It is appropriate to raise the point whether there is an ecological basis for requesting unimodal classes that are well separated. Grassland vegetation studies recommend 4 m² as an optimal sampling size for vegetation community description (Økland, 1990); the pixel size of the *casi* was 2 m by 2 m. The study showed that unimodal well-separated classes were not achieved at the management class level; at this level, the vegetation was neither uni-modal nor well separated. The test sites were, however, selected to represent areas that were homogeneous in terms of not only management but also species composition, and it was possible to achieve unimodal well-separated classes related to plant species composition within management classes. The scattergrams of data points along CDFs per test site showed only one data cloud per test site and we take this as an indication of the test site being homogeneous within the 30 m by 30 m area. It is thus considered ecologically reasonable to request unimodal spectral classes of natural vegetation when the natural variation is accounted for in a hierarchical approach.

Lewis (1994) performed a similar study of the relationship between ecological classification and spectral classification using hierarchical clustering and Landsat MSS data. The vegetation classification included registration of ground cover of the plant species and ground cover of plant litter, bare ground and stone. The vegetation classification in the thesis study included abundance scores for the different species but no information on plant litter, bare ground and stone. Lewis (1994) showed that ecological and spectral classes accounted for 42% of 38 test sites. In the thesis study, ecological and spectral classes

accounted for 82% of 18 test sites. The improved result may be due to the limited number of test sites compared to Lewis (*op cit*) but the excess number of bands and the high spatial resolution of the *casi* data compared to the MSS data are also likely to have influenced the result positively. Lewis (*op cit*) concludes that detection of subtle differences due to species characteristics was possible since major life form differences such as those between grassland and woodland were not present. This conclusion supports the results of the encroachment study, where it was found that spectral variation of grasslands was 'hiding' in the convex hull defined by coniferous forest, deciduous forest and shade.

The classification was performed for seven classes on nine spectral bands using ML classification. This was considered superior to a linear classifier of six CDFs (the maximum number of CDF in the case of seven classes) since the MNF analysis in the encroachment study showed that there was spectral signal in all nine MNFs. Thus data compression would have left out some important information - a point that was not made in Jacobsen et al. (2000b). Lewis (1998) detected and mapped nine vegetation classes based on 50 test sites and two Landsat TM scenes, applying the hierarchical clustering of vegetation as described above in Lewis (1994) and CDA for evaluation of the spectral separability of vegetation classes. The ML classification was likewise in the thesis study performed on original bands. The study of Lewis (1998) concluded that combination of ecological methods and sound image analysis was a valid way for spectral mapping of vegetation communities. The thesis study emphasised this conclusion and showed that it was possible to refine the spectral mapping with image data of increased spectral and spatial resolution.

Spectral unmixing as performed in the vegetation study was not considered a valid tool in this context since the mixture of the pixels was consisting of the same components (i.e. grassland vegetation, soil) regardless of plant community. The implication of this is that the plant communities would not be identified as endmembers in a convex geometry process (Jacobsen et al., 1998). In geometric terms the grassland spectra were 'hiding' in the convex hull expanded by the simplex defined by shade, conifers and deciduous forests. Image segmentation of grasslands and repetition of the end-to-end hyperspectral analysis would most likely have extracted new endmembers related to management treatments such as structure, coverage/patchiness, greenness, and distribution of soil and litter (Wessman et al., 1997). It is therefore unlikely that endmembers related directly to the MaFl classes would have been extracted since the classes are a combination of these factors – a fact that is especially acknowledged in the hierarchical approach.

The hierarchical approach developed took into consideration the nature of the remote sensing data and allowed for spectral identification at a plant community level. The method is not only applicable on dry grasslands. It is general in the sense of advocating a vegetation model adapted for remote sensing data by describing vegetation in terms of its three dimensions: structure, dynamics and taxonomy and a spectral model requiring that training classes can only be treated as spectral classes if they are spectrally well-defined.

Forest classification studies using the *casi* have shown that an overall classification accuracy for selected discriminant functions was increased from ~81 to ~90% using digital elevation data (Franklin, 1991). It is assumed that a higher level of calibration of image data would have optimised the classification but the digital elevation model (DEM) used in the georeferencing was not available until late in the study, and incorporation of topographic data in image calibration was therefore not within the scope of this project.

1.7.3 Georeferencing of end product

The TIN-based georeferencing method developed for this study made georeferencing possible to a higher level of accuracy than is possible using more standard image processing techniques such as polynomial surface modelling and it is seen as very valuable for any future work using airborne remote sensing data.

Polynomial models cannot, in general, be expected to georeference airborne scanner data satisfactorily. Airborne scanner data are subject to local distortions superimposed on medium to regional frequency distortions. TIN resampling, using automated selection of tie points from a DEM, identified local landscape features and therefore performed better than 3rd order polynomial modelling. Further TIN resampling has the benefit of improving poor correspondence in one area by inserting a new point in the area. Adding another GCP will also improve the resampled result using the regional approach. This will, however, most likely move the area of weak correspondence to another region. The drawback of TIN resampling is that only part of the image, inside the convex hull of tie points, can be resampled.

1.8 Conclusion on thesis project

The thesis contributes to its scientific field by developing methods for **i)** data quality assessment, and image atmospheric calibration, **ii)** environmental applications focusing on monitoring of encroachment stage and mapping of vegetation variation, and **iii)** georeferencing. As such, the thesis contributes to research with relation to airborne hyperspectral remote sensing and its implication for monitoring and mapping Danish semi-natural grasslands as is stated in the objective of the thesis project.

The data quality assessment study showed that care should be taken in airborne missions with respect to the performance standard of the imaging instrument. In the specific case of the *casi*, valuable information for spectral and radiometric calibration were more successfully obtained for the spectral data of contiguous spectra than the spatial data of discrete bands. It is recommended that this data type is acquired simultaneously with spatial mode data for, if nothing else, evaluation of data quality. The data quality assessment methods developed for this study is applicable for any hyperspectral scanner that is contiguously configured in narrow bands and is therefore valid for other studies involving commercial data where calibration quality is otherwise assessed with difficulty.

In general terms the time-consuming calibration issue may appear as a significant trade-off in terms of the application of airborne hyperspectral remote sensing, between the needs to pre-process the image data and those of using them in applications. It is instructive to note that a commercial operator, who went out of business soon after the flights, acquired the data collected during the DANMAC campaign with a poorly maintained scanner. Generally speaking, the *casi* is a well-performing instrument that is under constant development. The ITE[4] has invested in their own *casi* scanner and valuable research is being performed with *casi* data (see e.g. special issue of International Journal of Remote Sensing, vol. 18, no. 9, 1997). Thus there is little reason to be alarmed by the *casi* calibration problems encountered and resolved for in this study. The image processing for data quality of this study is nonetheless considered worthwhile since methods of general applicability were developed.

The method developed for atmospheric calibration of the spatial mode data, showed that field based measurements may be limited to one light reference target. The atmospheric calibration of the spatial mode data was based on a linear model and did not change the interdependency between pixels described by either their at-sensor radiance or their apparent surface reflectance. Application of reflectance spectra does, however, ensure that the image analysis is based on reflectance from the targets and not atmospheric effects. Furthermore, displaying and visual interpretation of reflectance spectra facilitate the work of the data analyst.

The implication studies showed that airborne hyperspectral remote sensing holds important potentials for ecological studies and monitoring of semi-natural grasslands. Examples of ecological studies of the importance of forests as the source of encroachment and monitoring of encroachment stage have been given as well as potentials for succession studies of plant communities. Both approaches may be developed further using data of higher spectral resolution covering a larger spectral range that allow for better application of hyperspectral techniques. The approach for encroachment stage mapping was based on a general approach for hyperspectral image analysis. The spectral identification of plant communities

---

[4]Institute of Terrestrial Ecology, Section for Earth Observation, National Environmental Research Council, Monkswood, the U.K. equivalent to National Environmental Research Institute.

was based on an analysis specifically developed with consideration to the superimposition of structural and dynamic variation on the spectral signal of vegetation. The developed method interpreted spectral variation with species composition based on canonical analysis of hyperspectral remote sensing data and gradient analysis of vegetation data. The method is recommended for further studies of vegetation classes with similar spectral signatures.

The georeferencing resolved the issue of attitude variation on the image geometry and georeferenced the image to an accuracy that facilitated use of ground reference data. The method developed showed that global polynomial distortion models valid for rigid satellite image are of less value in airborne images acquired from an unstable platform.

The study illustrated that data quality assessment, atmospheric calibration and georeferencing are important to studies of airborne data of high spatial and spectral resolution. It also illustrated the importance of the high flexibility of airborne scanners and that high spectral and spatial resolution data can provide ecological details of, for example. semi-natural grasslands, beyond what has been reported in the literature based on work with either satellite remote sensing multi-spectral data or traditional field-based methods. Furthermore, the study serves as an example of application of airborne missions to develop methods applicable with the future space borne satellite remote sensing systems. The thesis is a promising example of how satellites with increased spatial and spectral resolution might be used in environmental monitoring and mapping for conservation and research of protected habitats such as semi-natural grassland vegetation.

1.9 References

Asner, G.P. (1998): Biophysical and Biochemical Sources of Variability in Canopy Reflectance, Remote Sens. Environ. 64(3): 234-253.

Berk, A., L.S. Bernstein and C.C. Robertson (1989): MODTRAN: A Moderate Resolution Model for LOWTRAN 7, Final Report, GL-TR-0122, AFGL, Hanscom AFB, MA, 42p.

Blackburn, G.A. and E.J. Milton (1997): An Ecological Survey of Deciduous Woodlands Using Airborne Remote Sensing and Geographical Information Systems (GIS). Int. J. Remote Sensing, vol. 18, no. 9, pp.19191-1935.

Boardman, J.W. (1995): Analysis, Understanding and Visualization of Hyperspectral Data as Convex Sets in n-Space. SPIE, vol. 2480, pp. 14-22.

Boardman, J.W, F.A. Kruse, R.O. Green (1995). Mapping Target Signatures via Partial Unmixing of AVIRIS Data. Summaries of the Fifth Annual JPL Airborne Earth Science Workshop, January 23-26, vol. 1, AVIRIS Workshop.

Boardman, J.W. (1998): Convex Geometry and Mixing. In: Hyperspectral Data Analysis and Image Processing Workshop. Boulder, Colorado, 16-20 March. Analytical Imaging and Geophysics (AIG).

Broge, N.H., M. Hvidberg, B.U. Hansen, H.S. Andersen, A.A. Nielsen (1997): Analysis of Biophysical Relationships for a Wheat Canopy. Proceedings of the Third Airborne Remote Sensing Conference and Exhibition, vol. 2, pp. 373-379.

BSC (1997): Better Solutions Consulting. ENVI User's Guide, the Environment for Visualizing Images, Version 3.0. Internet http://www.rsinc.com.

Clark, R.N., G.A. Swayze, K.B. Heidebrecht, R.O. Green and A.F.H. Goetz (1995): Calibration to Surface Reflectance of Terrestrial Imaging Spectrometry Data: Comparison of Methods, Summaries of the Fifth Annual JPL Airborne Earth Science Workshop, vol. 1, pp 41-42.

Collins, W., S-H Chang, G. Rainse, F. Canney and R. Ashley (1983): Airborne Biogeophysical Mapping of Hidden Mineral Deposits. Economic Geology, vol. 78, pp. 737-749.

Conradsen, K., B.K. Nielsen and A.A. Nielsen (1991): Noise Removal in Multichannel Image Data by a Parametric Maximum Noise Fractions Estimator. In ERIM, Environmental Research Institute of Michigan (Eds.), Proceedings of the 24th International Symposium on Rem. Sens. Environ., pp. 403-416. Rio de Janeiro, Brazil.

Cortijo, F.J. and N.PD.L. Blanca (1997): A Comparative Study of Some Non-parametric Spectral Classifiers. Applications to Problems with High Overlapping Training Sets. Int. J. Remote Sensing, vol. 18, no. 6, 1259-1275.

CSES, Center for the Study of Earth from Space (1997): Atmospheric REMoval Program (ATREM), User's Guide, Version 3.0, Cooperative Institute for Research in Environmental Sciences (CIRES), University of Colorado, Boulder, 27 p.

Curran, P.J., J.L. Dungan, B.A. Macler, S.E. Plummer, D.L. Petersen (1992): Reflectance Spectroscopy of Fresh Whole Leaves for the Estimation of Chemical Concentration. Remote Sens. Environ., 39:153-166.

Curran, P.J., Kupiec, J.A., G.M. Smith (1998): Biochemical Composition of a Slash Pine Canopy. IEEE Transactions on Geoscience and Remote Sensing, vol. 35, no. 2, pp. 415-420.

Curtiss, B. and A.F.H. Goetz (1994): Field Spectrometry: Techniques and Instrumentation. Proc. International Symposium on Spectral Sensing Research, July, pp. 31-40.

Deering, D.W. (1989): Field Measurements of Bidirectional Reflectance. In: G. Asrar (Ed.): Theory and Applications of Optical Remote Sensing. John Wiley and Sons, Inc.

Devereux, B.J., R.M. Fuller, L. Carter, L., and R.J. Parsell (1990): Geometric Correction of Airborne Scanner Imagery by Matching Delaunay Triangles. Int. J. Remote Sensing, Vol. 11, no. 12, pp. 2237-2251.

Dwyer, J.L, Kruse, F.A., Lefkoff, A.B. (1995): Effects of Empirical Versus Model-Based Reflectance Calibration on Automated Analysis of Imaging Spectrometer Data: A Case Study from the Drum Mountains, Utah. Photogrammetric Engineering and Remote Sensing, vol. 61, no. 10, pp. 1247-1254.

Gamon, J.A., C.B. Field, D.A. Roberts, S.L. Ustin, R. Valentini (1993): Functional Patterns in an Annual Grassland during a AVIRIS Overflight. Remote Sens. Environ., 44:239-253.

Gao, B-C, A.F.H. Goetz (1990): Column Atmospheric Water Vapor and Vegetation Liquid Water Retrievals From Airborne Imaging Spectrometer Data. Journal of Geophysical Research, vol. 95, no. D4, pp. 3549-3564.

Gao, B-C, K.B. Heidebrecht, A.F.H. Goetz (1993): Derivation of Scaled Surface Reflectances from AVIRIS data, Remote Sens. Environ., 44:165-178.

Gates, D.M., H.J. Keegan, J.S. Schleter, V.R. Weidner (1965): Spectral Properties of Plants. Applied Optics, vol. 4, no. 1., pp. 11-20.

Gilabert, María Amparo, Soledad Gandía amd Meliá Joaquín (1996): Analysis of Spectral-Biophysical Relationships for a Corn Canopy. Remote Sens. Environ., 55:11-20.

Goetz, A.F.H. and W.M. Calvin (1987): Imaging Spectrometry: Spectral Resolution and Analytical Identification of Spectral Features. SPIE vol 834 Imaging Spectroscopy II, pp. 158-165.

Goetz, A.F.H., K.B. Heidebrecht (1996): Full-Scene, Subnanometer HYDICE Wavelength Calibration, Proceedings SPIE, Vol. 2821.

Goetz. A.F.H., Vane, G., J.E. Solomon, B.N. Rock (1985): Imaging Spectrometry for Earth Remote Sensing. Science, vol. 228, pp.1147-53.

Goetz, A.F.H., B. Kindel and J.W. Boardman (1996): Sub-pixel Target Detection in HYDICE Data from Cuprite, Nevada, Proceedings SPIE Annual Meeting, 2819, 7-14.

Goetz, A.F.H., Boardman, J.W., Kindel, B., Heidebrecht, K. (1997): Atmospheric Corrections: On Deriving Surface Reflectance from Hyperspectral Images. SPIE, San Diego, 28-30 July, vol. 3118, pp. 14-22.

Goetz, S.J. (1997): Multi-sensor Analysis of NDVI, Surface Temperature and Biophysical Variables at a Mixed Grassland Site. Int. J. Remote Sensing, vol. 18, no. 1, 77-94.

Graetz, D.R. (1990): Remote Sensing in Terrestrial Ecosystem Structure: An Ecologist's Pragmatic View. In, Remote Sensing of Biosphere Functioning, eds. R.J. Hobbs and H.A. Mooney. Ecological Studies, vol. 79, pp. 5-30.

Hoffbeck, J.P. and D.A. Landgrebe (1996): Classification of Remote Sensing Images Having High Spectral Resolution. Remote Sens. Environ. 57:119-126.

Iqbal, Mohammed (1983): An Introduction to Solar Radiation. Academic Press.

Jacobsen, A. (1995): Monitoring Climate Change in a Vegetated Arctic Environment, Zackenberg, North-eastern Greenland, Using Ground Truth Climatic Data and Remote Sensing. Geographica Hafniensia C3, Institute of Geography, University of Copenhagen. MSc-thesis. In Danish. ISSN No. 0908-6633. ISBN No. 87-87945-13-4.

Jacobsen, A. (1998): Monitoring Succession of Semi Natural Grasslands Using Convex geometry and Partial Unmixing. Unpublished.

Jacobsen, A., Broge, N.H. Hansen, B.U (1995): Monitoring Wheat Fields and Grasslands Using Spectral Reflectance Data. Proceedings of International Symposium on Spectral Sensing Research (ISSSR), Melbourne, Victoria, Australia, 26 Nov – 1 Dec. Available on CD-rom from Commonwealth Information Services, Australian Government Publishing Service, GPO Box 84, Canberra ACT 2601. ISBN No. 0 644 39625

Jacobsen, A., and B.U. Hansen (1996): Estimation of Soil Heat Flux/Net Radiation Ratio Over High Latitude Natural Vegetation Using Spectral Vegetation Indices. Proceedings of Fourth Circumpolar Symposium on Remote Sensing of the Polar Environments, TUD, Lyngby, Denmark, 29 April - 1 May. ESA SP-391, July 1996. Pp. 33-38.

Jacobsen, A., and B.U. Hansen (1999): Estimation of the Soil Heat Flux/Net Radiation Ratio from Spectral Vegetation Indices in High Latitude Arctic Areas. Int. J. Remote Sensing, vol. 20, no. 2. Pp. 445-461.

Jacobsen, A., K.B. Heidebrecht, A.F. Goetz (2000a): Assessing the Quality of the Radiometric and Spectral Calibration of *casi* Data and Retrieval of Surface Reflectance Factors. Photogrammetric Engineering and Remote Sensing, vol. 66, no. 1, pp. 1083-1091.

Jacobsen, A., K.B. Heidebrecht, A.A. Nielsen (1998): Monitoring Grasslands Using Convex Geometry and Partial Unmixing – a Case Study. Proceedings of 1st EARSel Workshop on Imaging Spectroscopy, Remote Sensing Laboratories, University of Zürich, Switzerland, 6-8 October. Eds. Michael Shaepman, Daniel Schläpfer, Klaus Itten. Pp. 309-316.

Jacobsen, A., A.A. Nielsen, R. Ejrnæs, G. Groom (1999a): Spectral Identification of Danish Grassland Classes Related to Management and Plant Specie Composition. Proceedings of 4th International Airborne Remote Sensing Conference and Exhibition, Ottawa, Canada, 21-24 June, vol I, pp74-81.

Jacobsen, A., A.A. Nielsen, R. Ejrnæs, G. Groom (2000b): Monitoring Grasslands through Spectral Identification of Plant Communities. Canadian Journal of Remote Sensing., 21-24 June, vol. 26, no.5, pp. 370-383.

Jacobsen, A., N. Drewes, M. Stjernholm, T. Balstrøm (1999b): Generation of a Digital Elevation Model of Mols Bjerge, Denmark, and Georeferencing of Airborne Scanner Data. Danish Journal of Geography, pp. 35-46.

Kent, M. and P. Coker (1992): The Nature of Quantitative Ecology and Vegetation Science. In, Vegetation Description and Analysis. A Practical Approach, pp. 1-28.

Kruse, F.A. Lefkoff, A.B., J.B. Dietz (1993a): Expert System-based Mineral Mapping in Northern Dead Valley, California/Nevada, Using Airborne Visible/Infrared Imaging Spectrometer (AVIRIS). Remote Sens. Environ., 44:309-336.

Kruse F.A., A.B. Leffkoff, J.W. Boardman, K.B. Heidebrecht, A.T. Shapiro, P.J. Barloon, and A.F.H. Goetz (1993b): The Spectral Image Processing System (SIPS) – Interactive Visualization and Analysis of Imaging Spectrometer Data. Remote Sens. Environ. 44: 145-163.

Kruse, F.A. (1994): Imaging Spectrometer Data Analysis – A Tutorial, Proceeding of International Symposium on Spectral Sensing Research (ISSSR), 10-15 June, San Diego, CA, vol I, pp. 44-54.

Lauver, C.L. and J.L. Whistler (1993): A Hierarchical Classification of Landsat TM Imagery to Identify Natural Grassland Areas and Rare Species Habitat. Photogrammetric Engineering and Remote Sensing, vol. 59, no. 5, pp. 627-634.

Larsen, R., , A.A. Nielsen and K. Conradsen (1998). Restoration of Hyperspectral Push-broom Scanner Data. In P. Gudmandsen (Ed.) Proceedings of the 17th EARSEL Symposium on Future Trends in Remote Sensing, pp. 157-162, Lyngby, Denmark, 17-19 June 1997. Balkema, Rotterdam, ISBN 90 54 10 533 5.

Lewis, M.M. (1994): Species Composition Related to Spectral Classification in an Australian Spinifex Hummock Grassland. Int. J. Remote Sens., vol 15, no.16, pp. 3223-3239.

Lewis, M.M. (1998): Numeric Classification as an Aid to Spectral Mapping of Vegetation Communities. Plant Ecology, vol. 136, pp. 133-149.

Lobo, A., K. Moloney, and N. Chiariello (1998): Int. J. Remote Sensing, vol. 19, no. 1, 65-84.

McCloy, K. (Ed.) (1997): DANMAC - DANish Multisensor Airborne Campaign. Status Report.

McCloy, K. (Ed.) (1999): DANMAC. - DANish Multisensor Airborne Campaign. Final Report 1996-1998.

Mitchell, J.F.B. (1989): The "Greenhouse" Effect and Climate Change. Rev. Geophys, vol. 27, no .1, pp. 115-139.

Niblack, W. (1985): An Introduction to Digital Image Processing. Strandberg Publishing Company, 3460 Birkeroed, Denmark. ISBN 87-872-0055-4.

Nielsen, A.A and R. Larsen (1994): Restoration of GERIS data Using the Maximum Noise Fractions Transform. In ERIM, Environmental Research Institute of Michigan (Ed.), Proceedings of The First International Airborne Remote Sensing Conference and Exhibition, Strasbourg, France, 11-15 September 1994, pp. 557-568.

Peñuelas, J, I. Filella, C. Biel, L. Serrano, R. Savé (1993): The Reflectance at the 950-970 Region as an Indicator of Plant Water Status. Int. J. Remote Sensing, vol. 14, no. 10, pp. 1887-1905.

Philpot, W.D. (1991): The Derivative Ratio Algorithm: Avoiding Atmospheric Effects in Remote Sensing. IEEE Transactions on Geoscience and Remote Sensing 29(3): 350-357.

Ray T.W. and B.C. Murray (1996): Nonlinear Spectral Mixing in Desert Vegetation. Remote Sens. Environ. 55: 59-64.

Resmini, R. G., Kappus, M. E., Aldrich, W. S., Harsanyi, J. C. and Anderson, M. Mineral Mapping with HYperspectral Digital Imagery Collection Experiment (HYDICE) Sensor Data at Cuprite, Nevada, U.S.A. Int. J. Remote Sensing, 18(7):1553-1570.

Richards, J.A. (1993): Remote Sensing Digital Image Analysis. An Introduction. Second Revised and Enlarged Edition. ISBN 3-540-58219-3 2nd Ed. Springer Verlag Berlin Heidelberg New York.

Rollin E.M. and E.J. Milton (1998): Processing of High Spectral Resolution Reflectance Data for the Retrieval of Canopy Water Content Information. Remote Sens. Environ. 65: 86-92.

Rouse, Jr., J. W., R. Haas, D.W. Deering, J.A. Schell, J.C. Harlan (1974): Monitoring the Vernal Advancement and Retrogradation (Green Wave Effect) of Natural Vegetation. NASA/GSFC Type III Final Report, Greenbelt, MD, 371.

Rubin, Tod (1997): Airborne Imaging Spectrometry in Practice. ERIM Airborne Remote Sensing Conference, Copenhagen.

Skriver, Henning (Ed.) (1996): DANMAC. Danish Multisensor Airborne Campaign. Status Report 1996.

Schowengerdt, R.A. (1997): Remote Sensing. Models and Methods for Image Processing. 2nd ed. Academic Press. San Diego.

Scot Conseil and Smith System Engineering (1992): Use of Satellite Data for Environmental Purposes in Europe. A Study for the European Commission. Study Contract No. ETES-0039-D.

Singhroy, H.V. and F.A. Kruse (1991): Detection of Metal Stress in Boreal Forest species Using the 0.67 μm Chlorophyll Absorption Band. Proc. Eighth Thematic Conference on Geologic Remote Sensing, Exploration, Engineering and Environment, Denver, Colorado, 29 April – 2 May.

Stoner, W. and R. Resmini (1996): Hyperspectral Remote Sensing. SAIC Science and Technology Paper. Http://www.saic.com:80/Publications/techtrends/stonerab.html.

Swain, P.H. and S.M. Davis (eds.) (1978): Remote Sensing: The Quantitative Approach. Chapt. 3, pp. 136-187. New York, NY: McGraw-Hill.

Tod, S.W., R.M. Hoffer, and D.G. Milchunas (1998): Biomass Estimation on Grazed and Ungrazed Rangelands using Spectral Indices. Int. J. Remote Sensing, vol. 19, no. 3, 427-438.

Tompkins, S., J.F. Mustard, C.M. Pieters, and D.W. Forsyth (1997): Optimization of Endmembers for Spectral Mixture Analysis. Remote Sens. Environ. 59:472-489.

Tychsen, J. M. Olsen, K. Rasmussen, H. Skriver, P. Gudmandsen (1994): Environmental Monitoring by Remote Sensing. Background Report, Final Edition. Insitute of Geography, University of Copenhagen. ISBN no. 87-87945-08-8.

Vane, G., A.F.H.Goetz (1993): Terrestrial Imaging Spectrometry: Current Status, Future Trends. Remote Sensing Environ., 44:117-126.

Wessman, C.A. (1994): Estimation Canopy Biochemistry through Imaging Spectrometry. In: J. Hill and J. Mégier (eds.): Imaging Spectrometry – a Tool for Environmental Observations, pp. 57-69.

Wessman, C.A., C.A. Bateson, T.L. Benning, (1997): Detecting Fire and Grazing Patterns in a Tallgrass Prairie Using Spectral Mixture Analysis, Ecological Applications, 7:493-511.

Wilson, A.K. (1994): The NERC Integrated ATM/*casi*/GPS System. First International Airborne Remote Sensing Conference and Exhibition, Strasbourg, France, 11-15 September, vol II, pp. 249-259.

Wooley, J.T. (1971): Reflectance and Transmittance of Light by Leaves. Plant Physiol., vol. 47, pp. 656-662.

Økland, R.H. 1990. "Vegetation Ecology: Theory, methods and applications with reference to Fennoscandia", *Sommerfeltia* suppl. Vol. 1.

2. Articles

2.1 Introduction to articles

The articles of the thesis, given in summary in Sections 1.6 to 1.9, are covered in 2 published conference proceedings and 3 published refereed national and international articles. The full references are given below in order of appearance. The pilot study is included as article VI.

Article I:

Assessing the Quality of the Radiometric and Spectral Calibration of CASI data and Retrieval of Surface Reflectance Factors by A. Jacobsen, K.B. Heidebrecht and A.F.H. Goetz. Photogrammetric Engineering and Remote Sensing, vol. 66, no. 1, pp. 1083-1091.

The article was presented at the Center for the Study of Earth from Space (CSES), University of Colorado at Boulder, CO USA and at a DANMAC seminar of 18 August 1998.

Article II:

Monitoring Grasslands using Convex Geometry and Partial Unmixing – a Case Study by A. Jacobsen, K.B. Heidebrecht and A.A. Nielsen. Schaepman, M., D. Schläpfer and K. Itten (eds.): 1st EARSeL Workshop on Imaging Spectroscopy, Remote Sensing Laboratories, University of Zurich, Switzerland, 6-8 October 1998, pp. 309-316.

The proceedings paper was presented at Center for the Study of Earth from Space (CSES), University of Colorado at Boulder, at the oral session Land Cover Monitoring on the above mentioned Workshop and at the DANMAC seminar of 18 August 1998.

Article III:

Spectral Identification of Danish Grasslands Classes Related to Management and Plant Species Composition by A. Jacobsen, A.A. Nielsen, R. Ejrnæs and G.B. Groom. Proceedings of the Fourth International Remote Sensing Conference and Exhibition, 21-24 June 1999, Ottawa, Ontario, Canada, vol. I, pp. 74-81.

The proceedings paper was presented at the interactive poster and oral sessions Land Cover/Land Use at the above mentioned Conference. The poster was awarded a Best of Session Award.

Article IV:

Spectral Identification of Plant Communities for Mapping of Semi-Natural Grasslands by A. Jacobsen, A.A. Nielsen, R. Ejrnæs and G.B. Groom. Canadian Journal of Remote Sensing, vol. 26, no.5, pp. 370-383.

This article is closely related to the previous conference contribution that was invited to the special conference issue of Canadian Journal of Remote Sensing. As such, the core of the conference contribution has been maintained and new interesting findings have been added. The sections of spectral and vegetation analysis are merely the same whereas the image classification section is new to this paper. Some errors in field and vegetation classifications with effects on the spectral identification were identified and corrected.

Article V:

Generation of a Digital Elevation Model of Mols Bjerge, Denmark, and Georeferencing of Airborne Scanner Data by A. Jacobsen, N. Drewes, M. Stjernholm and T. Balstrøm. Danish Journal of Geography, vol. 99, pp. 35-46.

The article was presented at the DANMAC seminar of 4 December 1998.

Article VI:

Monitoring Wheat Fields and Grasslands Using Spectral Reflectance Data Field Spectra of Grassland Vegetation by A. Jacobsen, N. Broge and B.U. Hansen. Proceedings of International Symposium on Spectral Sensing Research (ISSSR), Melbourne, Victoria, Australia, 26 Nov – 1 Dec. Available on CD-rom from Commonwealth Information Services, Australian Government Publishing Service, GPO Box 84, Canberra ACT 2601. ISBN No. 0 644 39625.

The proceedings paper was presented as an interactive poster at the Conference in session of Terrestrial and Land Surface Studies and Applications.

The following pages paginated I-VI are division pages between the articles. The articles are paginated separately within the division pages.

National Environmental Research Institute

The National Environmental Research Institute, NERI, is a research institute of the Ministry of Environment and Energy. In Danish, NERI is called *Danmarks Miljøundersøgelser (DMU)*.
NERI's tasks are primarily to conduct research, collect data, and give advice on problems related to the environment and nature.

Addresses: URL: http://www.dmu.dk

National Environmental Research Institute   *Management*
Frederiksborgvej 399   *Personnel and Economy Secretariat*
PO Box 358   *Research and Development Section*
DK-4000 Roskilde   *Department of Atmospheric Environment*
Denmark   *Department of Environmental Chemistry*
Tel: +45 46 30 12 00   *Department of Policy Analysis*
Fax: +45 46 30 11 14   *Department of Marine Ecology*
                                                                         Department of Microbial Ecology and Biotechnology
                                                                         Department of Arctic Environment

National Environmental Research Institute   *Environmental Monitoring Co-ordination Section*
Vejlsøvej 25   *Department of Lake and Estuarine Ecology*
PO Box 314   *Department of Terrestrial Ecology*
DK-8600 Silkeborg   *Department of Streams and Riparian areas*
Denmark
Tel: +45 89 20 14 00
Fax: +45 89 20 14 14

National Environmental Research Institute   *Department of Landscape Ecology*
Grenåvej 12-14, Kalø   *Department of Coastal Zone Ecology*
DK-8410 Rønde
Denmark
Tel: +45 89 20 17 00
Fax: +45 89 20 15 15

Publications:
NERI publishes technical reports, technical instructions, and the annual report. An R&D project catalogue is available in an electronic version on the World Wide Web.
Included in the annual report is a list of the publications from the current year.

This PhD thesis contributes to its scientific field by developing methods for **i)** data quality assessment, and image atmospheric calibration, **ii)** environmental applications focusing on monitoring of encroachment stage and mapping of vegetation variation, and **iii)** georeferencing. As such, the thesis contributes to research with relation to airborne hyperspectral remote sensing and its implication for monitoring and mapping Danish semi-natural grasslands.